C.A. Yan, R. Vescovini, E.L. Jansen
A Semi-Analytical Framework for Nonlinear Vibration Analysis of Variable Stiffness Plates
Composite Structures, In press - Published online 20/04/2021
doi:10.1016/j.compstruct.2021.113954

A Semi-Analytical Framework for Nonlinear Vibration Analysis of Variable Stiffness Plates

C.A. Yan[1], R. Vescovini[1]*and E.L. Jansen[2]

[1] *Dipartimento di Scienze e Tecnologie Aerospaziali, Politecnico di Milano*

Via La Masa 34, 20156 Milano, Italy

[2] *Rotterdam University of Applied Sciences*

G.J. de Jonghweg 4-6, 3015 GG Rotterdam, Netherlands

Abstract

Focus of this paper is the development of a fast semi-analytical framework to address the nonlinear vibration response of plates with Variabile Stiffness (VS) configuration. A formulation is developed based on a mixed variational theorem. A Ritz-like approach is employed for handling the spatial dependence, whilst several techniques are developed and compared for the temporal dependence: the method of averaging, a perturbation approach, an iterative procedure based on the Harmonic Balance Method (HBM) and a direct integration method. The proposed framework allows fast parametric studies to be performed for assessing the nonlinear vibration response of VS plates. The comparison against reference results demonstrates the validity of the proposed formulations in capturing the nonlinear free and forced responses with relative computational ease. This aspect is further exploited by presenting parametric studies, where the role of fiber path and boundary conditions is assessed. These studies aim at providing further understanding into the underlying mechanical response and illustrate the potential of the proposed semi-analytical approaches as a valuable mean to assist the design of VS plates.

Keywords: Nonlinear vibrations; Semi-analytical methods; Variable Stiffness composites.

1 Introduction

An emerging and promising class of composite laminates relies upon the variable stiffness (VS) concept; the idea dates back to the late sixties [1], although just recently the development of key technologies, such as automated fiber placement and continuous tow shearing, are making these solutions potential candidates for the structures of the next generation. In VS laminates, stiffness properties are not constant along the

*Corresponding author. *Email address:* riccardo.vescovini@polimi.it (Riccardo Vescovini)

in-plane directions, but can be tailored to meet design requirements with improved efficiency. A possible way to achieve stiffness variability consists in allowing fibers to run along curvilinear paths, with orientation angles varying according to different laws. Linear variations [2], Lagrange [3, 4], Lobatto [5] and piecewise polynomials [6] are few but examples of common choice employed to describe the fiber path. The effects of fiber misalignment due to the manufacturing processes were recently investigated by Pagani and Sanchez-Majano [7, 8]. The advantages of VS structures are manifold, ranging from improved buckling [2, 9, 10] and post-buckling response [11, 12] to enhanced bending [13], thermal performance [14, 15, 16], and damage resistance [17]. Potential advantages exist even in terms of nonlinear vibration behaviour [18], although relatively less attention has been devoted in the literature to this aspect. Space applications could particularly benefit from improved nonlinear vibration response, as they are commonly realized with thin panels forced to vibrate at large amplitude by their operating environment. It is not by chance that early works in the field of nonlinear vibrations date back to the fifties, with growing interest especially in the early stages of space era [19].

Many strategies have been proposed in the years, combining different strategies for handling the spatial and time dependence of the equations governing the nonlinear, dynamic equilibrium [20]. A comprehensive review of the topic can be found in Ref. [21]. Early works focused on the analytical approach to the subject, referring to elliptic functions [22], Galerkin method [23] and Navier-type expansion [24, 25] for the spatial part; perturbation-like approaches were employed for dealing with the problem time-dependency. While advantageous from a computational perspective, analytical solutions are generally restricted to specific configurations, both in terms of material properties and boundary conditions.

In general, these restrictions can be overcome referring to the Finite Element Method (FEM). Early attempts are found in Ref. [26] and, since then, numerous investigations have been carried out. The direct integration scheme of Ref. [27] and the application of the Harmonic Balance Method (HBM) of Refs. [28, 29] are few but examples of FEM-based procedures for nonlinear vibration problems. Despite inherent accuracy and versatility, standard FE procedures are generally characterized by relatively large number of degrees of freedom, this feature being undesirable when multiple nonlinear analyses must be run, such as in case preliminary optimizations or parametric studies. Attempts to mitigate these restrictions promoted the use of the p-version of the FEM, the main idea consisting in adopting higher-order shape functions, which, in turn, allows coarser meshes to be used. In this context, the work of Refs. [30, 31, 32] are worth of mention, the first focusing on isotropic plates, the two others on VS configurations; time dependence is taken care of using the HBM method.

Other attempts to keep the computational burden at minimum focused on semi-analytical techniques, where equations are derived analytically, while their solution is sought numerically. In many cases, these models can be understood as a single-domain FEM p-version, although the expansion is not necessarily polynomial, as it is most common in FEM.

In this context, applications of Galerkin-like approaches are developed in Refs. [33, 34]. Prabhakar and Chia [33] proposed the use of eigenbeam functions and HBM, while the technique of Ref. [34] relies upon a two-mode trigonometric expansion and the method of averaging. A similar approach is adopted in more recent works due to Amabili [35], where use is made of a mathematical software to manipulate the analytical expressions of the governing equations which are then solved numerically through direct integration and an arc-length method. The Galerkin method in combination with the method of averaging and a Fourier semi-discretization in combination with a perturbation approach were proposed by Jansen [36] for analyzing the nonlinear vibrations of cylindrical shells.

Starting from this background, this paper aims at extending the current semi-analytical capabilities to address nonlinear vibrations of VS plates. Earlier works have focused on p-FEM approaches [18, 31, 13], while semi-analytical strategies are relatively scarce, and are believed of crucial importance for maximizing the efficiency of the analysis process. This aspect is of particular interest for handling VS configurations, where several design variables need to be handled and more tailoring opportunities are available. Furthermore, the underlying structural behaviour of VS plates is inherently complex, thus simple analysis methods allow deeper understanding of the mechanical response to be gathered. With this purposes in mind, a formulation based on the combined use of a mixed approach [37, 38, 39] and the Ritz method is developed. This approach is an extension of the post-buckling formulations presented earlier in Refs. [39, 12] to the case of nonlinear vibration analysis. To the best of the authors' knowledge, no previous attempts can be found in the literature to face the nonlinear vibrations of VS plates with a similar procedure.

A second goal of this work consists in presenting different strategies for solving the ordinary differential equations arising from the spatial discretization. Most of the work in the literature focus on specific implementations, while comparison among different approaches for handling the time-dependence are quite rare and believed of interest. For this scope, four methods are considered here, i.e. the method of averaging, a perturbation procedure analogous to Koiter's initial postbuckling theory, iterative procedures based on the HBM and a direct time integration approach. The four methods are compared in terms of computational time and accuracy of predictions.

The paper is organized as follows: Section 2 provides the theoretical background to the formulation, presenting the variational framework and the semi-discretization of the governing partial differential equations via Ritz approximation; Section 3 is devoted to the description of the methods for solving the ordinary differential equations resulting from the Ritz approximation. Four strategies are presented for this scope; the results are discussed in Section 4. Firstly, the comparison against literature results is presented, then parametric studies are conducted to illustrate a potential use of the formulation developed here.

2 Formulation

In this section, a formulation is presented for the analysis of thin composite plates obtained by the stacking of plies with curvilinear fibers. With no loss of generality, the fiber angles are assumed to exhibit linear variation along an arbitrary direction. Referring to Figure 1, the function expressing the fiber angle as a function of x' is given by [10]:

$$\theta(x') = \phi + (T_1 - T_0)\frac{|x'|}{d} + T_0 \tag{1}$$

where ϕ is the angle between the reference path and the x axis, while T_0 and T_1 are the angles at the reference points A and B, respectively. In the formulation presented hereinafter, the point A is taken to be at the center of the plate, while B is taken at a characteristic distance d from A by moving along x'. Each layer is specified through the compact notation $\phi\langle T_0|T_1\rangle$, while the laminate as a whole by $\left[\phi^1\langle T_0^1|T_1^1\rangle, \phi^2\langle T_0^2|T_1^2\rangle, ..., \phi^{N_\mathrm{p}}\langle T_0^{N_\mathrm{p}}|T_1^{N_\mathrm{p}}\rangle\right]$. In this notation, the superscripts are the ply-related indices, and N_p is the number of plies composing the laminate.

Still referring to Figure 1, a Cartesian coordinate system is taken over the plate midsurface, whose origin is located at the center of the plate. The x and y axes run along the longitudinal and the transverse direction, respectively, while the z axis is obtained to form a right-handed system. For future developments, it is useful to introduce the nondimensional coordinates ξ and η, defined as $\xi = \frac{2}{a}x$, $\eta = \frac{2}{b}y$, where a and b denote the longitudinal and the transverse dimensions, respectively. The total laminate thickness is h.

The in-plane conditions are those of movable – edges free to move, but forced to remain straight –, immovable or free edges, a summary of which is reported in Figure 1(a); any flexural boundary condition can be considered, i.e. free (F), simply-supported (S) and clamped (C) – see Figure 1(b). Owing to the inherent nonlinear coupling between in-plane and out-of-plane response, any problem requires the combined definition of both flexural and in-plane conditions.

Following von Kármán nonlinear thin plate theory [40], the strain–displacement relation is given in the form:

$$\boldsymbol{\epsilon} = \boldsymbol{\epsilon}_0 + z\mathbf{k} \tag{2}$$

where the vector of strains is $\boldsymbol{\epsilon} = \{\epsilon_{xx}\ \epsilon_{yy}\ \gamma_{xy}\}^\mathrm{T}$, while the membrane strains $\boldsymbol{\epsilon}_0$ and plate curvatures $\mathbf{k}$ are defined as:

$$\boldsymbol{\epsilon}_0 = \left\{u_{,x} + \tfrac{1}{2}w_{,x}^2 \quad v_{,y} + \tfrac{1}{2}w_{,y}^2 \quad u_{,y} + v_{,x} + w_{,x}w_{,y}\right\}^\mathrm{T} \qquad \mathbf{k} = \left\{-w_{,xx} \quad -w_{,yy} \quad -2w_{,xy}\right\}^\mathrm{T} \tag{3}$$

In Eq. (3), u, v and w are the middle surface displacement components along the three coordinate directions; the comma followed by an index denotes differentiation with respect to that index.

The assumption of symmetric layup is introduced, as most of laminates used in real applications are so. In

this case, the semi-inverse constitutive law is block-wise diagonal and reads:

$$\begin{Bmatrix} \boldsymbol{\epsilon}_0 \\ \mathbf{M} \end{Bmatrix} = \begin{bmatrix} \mathbf{a}(x,y) & \mathbf{0} \\ \mathbf{0} & \mathbf{D}(x,y) \end{bmatrix} \begin{Bmatrix} \mathbf{N} \\ \mathbf{k} \end{Bmatrix} \tag{4}$$

with $\mathbf{a}$ and $\mathbf{D}$ denoting the in-plane compliance and bending stiffness matrices available from Classical Lamination Theory (CLT), while $\mathbf{N} = \{N_{xx}\ N_{yy}\ N_{xy}\}^{\mathrm{T}}$ and $\mathbf{M} = \{M_{xx}\ M_{yy}\ M_{xy}\}^{\mathrm{T}}$ are the vectors collecting the stress and moment resultants [40].

The formulation is developed by referring to a mixed variational approach, where the unknowns of the problem are the out-of-plane deflection w and the Airy stress function F, the latter defined as:

$$F_{,yy} = N_{xx} \quad F_{,xx} = N_{yy} \quad F_{,xy} = -N_{xy} \tag{5}$$

The stress function F allows the in-plane equilibrium equations to be identically satisfied. The problem is then reduced to the fulfillment of the out-of-plane equilibrium and the in-plane compatibility requirements. In this work, these two conditions are enforced in a weak-form by referring to the unified variational principle due to Giavotto [37, 41]:

$$\begin{aligned} \Pi^* = &-\frac{1}{2}\int_{\mathrm{S}} \mathbf{F}^{\mathrm{T}}\mathbf{a}\mathbf{F}\,\mathrm{dS} + \frac{1}{2}\int_{\mathrm{S}} \mathbf{k}^{\mathrm{T}}\mathbf{D}\mathbf{k}\,\mathrm{dS} + \frac{1}{2}\int_{\mathrm{S}} \left(F_{,yy}w_{,x}^2 - 2F_{,xy}w_{,x}w_{,y} + F_{,xx}w_{,y}^2\right)\,\mathrm{dS} + \\ &+ \frac{1}{2}\int_{\mathrm{S}} I_0\dot{w}^2\,\mathrm{dS} - \int_{\mathrm{S}} wq\,\mathrm{dS} \end{aligned} \tag{6}$$

where the second derivatives of the stress function F are collected in the vector $\mathbf{F} = \{F_{,yy}\ F_{,xx}\ -F_{,xy}\}^{\mathrm{T}}$, while I_0 is the inertia term corresponding to the out-of-plane displacement and q the external load in the form of a pressure; the dot denotes differentiation with respect to time. By application of the techniques of variational analysis, it is straightforward to demonstrate that the Euler-Lagrange equations of Eq. (6) are indeed the dynamic out-of-plane equilibrium and the compatibility equations [42]. The weak-form formulation of the problem as per Eq. (6) is particularly suited for applying direct solution techniques, such as the Ritz method. For this reason, this is the approach pursued here.

It is worth noting that the effects of in-plane and rotary inertia are not included in Eq. (6). Indeed they can be reasonably assumed to be negligible for most thin plate applications, especially when flexural vibrations in the low/mid frequency range are of concern.

The Hamilton principle, $\int_{t_1}^{t_2} \delta\Pi^*\,\mathrm{d}t = 0$, is imposed after introducing the Ritz method. With this purpose, Legendre polynomials L_i are used for expanding the problem's unknowns. Specifically, their expression reads:

$$L_i(x) = \sum_{j=0}^{J} (-1)^j \frac{(2i-2j)!}{2^i j!(i-j)!(i-2j)!} x^{i-2j} \quad \text{with:} \quad J = \begin{cases} \frac{i}{2} & \text{if } i = 0, 2, 4... \\ \frac{i-1}{2} & \text{if } i = 1, 3, 5... \end{cases} \tag{7}$$

Following Wu et al.[39, 43], the Airy stress function is conveniently expressed as:

$$F(\xi,\eta) = F_0(\xi) + F_1(\eta) + F_2(\xi,\eta) \tag{8}$$

where a split is operated between the terms representing the membrane force resultants at the boundaries, i.e. F_0 and F_1, and those inside the domain, i.e. F_2. Specifically, the first two terms are expanded as:

$$\begin{aligned} N_{yy}(\xi) &= \frac{4}{a^2} F_{0,\xi\xi}(\xi) = \frac{4}{a^2} \sum_{j=\alpha}^{J} d_j L_j(\xi) \\ N_{xx}(\eta) &= \frac{4}{b^2} F_{1,\eta\eta}(\eta) = \frac{4}{b^2} \sum_{k=\alpha}^{K} c_k L_k(\eta) \end{aligned} \tag{9}$$

The coefficient α in the summatories above is chosen according to the in-plane boundary conditions at the edges, which can be movable ($\alpha = 1$) or immovable ($\alpha = 0$) [39]. Free in-plane edges are retrieved by dropping the terms F_0 and F_1 from Eq. (8).

The contribution F_2 of Eq. (8) – the one describing the membrane stress distribution in the plate domain – is expressed as:

$$F_2(\xi, \eta) = \sum_{pq=0}^{PQ} \Phi_{pq} X_p(\xi) Y_q(\eta) \tag{10}$$

where $X_p(\xi)$ and $Y_q(\eta)$ are obtained as:

$$X_p(\xi) = (1-\xi^2)^2 L_p(\xi), \quad Y_q(\eta) = (1-\eta^2)^2 L_q(\xi) \tag{11}$$

Accordingly, the out-of-plane deflection is expanded as:

$$w(\xi, \eta) = \sum_{mn=0}^{MN} w_{mn} \overline{X}_m(\xi) \overline{Y}_n(\eta) \tag{12}$$

where the polynomial series along the longitudinal and the transverse directions are obtained as the product between boundary functions and Legendre polynomials:

$$\overline{X}_m(\xi) = (1+\xi)^{i1}(1-\xi)^{j1} L_m(\xi), \quad \overline{Y}_n(\eta) = (1+\eta)^{i2}(1-\eta)^{j2} L_n(\eta) \tag{13}$$

The coefficients i_k and j_k are introduced to guarantee the fulfillment of the essential boundary conditions. In particular, they are taken as 0, 1 and 2 for free (F), simply supported (S) and clamped (C) conditions, respectively.

Upon substitution of Eqs. (8)-(12) into Eq. (6), the approximation of the functional Π^* is obtained as:

$$\begin{aligned} \Pi^* = &\frac{1}{2}\left(d_j S^{dd}_{(j)(\overline{j})} d_{\overline{j}} + c_j S^{cc}_{(k)(\overline{k})} c_{\overline{k}} + \Phi_{pq} S^{\Phi\Phi}_{(pq)(\overline{pq})} \Phi_{\overline{pq}} \right) + c_k S^{cd}_{(k)(j)} d_j + \Phi_{pq} S^{\Phi d}_{(pq)(j)} d_j + \Phi_{pq} S^{\Phi c}_{(pq)(k)} c_k + \\ &+ \frac{1}{2} w_{mn} \left(K^{ww}_{(mn)(\overline{mn})} + \tilde{\mathcal{N}}_{(j)(mn)(\overline{mn})} d_j + \hat{\mathcal{N}}_{(k)(mn)(\overline{mn})} c_k + \mathcal{N}_{(pq)(mn)(\overline{mn})} \Phi_{pq} \right) w_{\overline{mn}} + \\ &+ w_{mn} M^{ww}_{(mn)(\overline{mn})} \ddot{w}_{\overline{mn}} + w_{mn} P^{w}_{\overline{mn}} \end{aligned} \tag{14}$$

Use is made here of the notation presented in Ref. [12], where vectors are denoted as $a_i = \mathbf{a}$, matrices as $A_{(i)(r)} = \mathbf{A}$ and arrays of matrices as $A_{(i)(r)(m)} = \boldsymbol{\mathcal{A}}_i$. Note, the approximation of Π^* as per Eq. (14)

requires the evaluation of the surface integrals implied by Eq. (6), which are performed numerically via Gauss integration. The explicit form of these terms is reported in the Appendix.
The Hamilton's principle is imposed by taking the partial derivatives of Eq. (14) with respect to the Ritz amplitudes c_k, d_j, Φ_{pq} and w_{mn}, leading to the following system of ordinary differential equations in the time variable:

$$\begin{cases} \frac{\partial \Pi^*}{\partial \mathbf{d}}: & \mathbf{S}^{dd}\mathbf{d} + \mathbf{S}^{dc}\mathbf{c} + \mathbf{S}^{d\Phi}\mathbf{\Phi} + \frac{1}{2}\mathbf{w}^{\mathrm{T}}\tilde{\boldsymbol{\mathcal{N}}}_j\mathbf{w} = \mathbf{0} \\ \frac{\partial \Pi^*}{\partial \mathbf{c}}: & \mathbf{S}^{cd}\mathbf{d} + \mathbf{S}^{cc}\mathbf{c} + \mathbf{S}^{c\Phi}\mathbf{\Phi} + \frac{1}{2}\mathbf{w}^{\mathrm{T}}\hat{\boldsymbol{\mathcal{N}}}_k\mathbf{w} = \mathbf{0} \\ \frac{\partial \Pi^*}{\partial \mathbf{\Phi}}: & \mathbf{S}^{\Phi d}\mathbf{d} + \mathbf{S}^{\Phi c}\mathbf{c} + \mathbf{S}^{\Phi\Phi}\mathbf{\Phi} + \frac{1}{2}\mathbf{w}^{\mathrm{T}}\boldsymbol{\mathcal{N}}_{pq}\mathbf{w} = \mathbf{0} \\ \frac{\partial \Pi^*}{\partial \mathbf{w}}: & \mathbf{M}^{ww}\ddot{\mathbf{w}} + \mathbf{K}^{ww}\mathbf{w} + \mathbf{d}^{\mathrm{T}}\tilde{\boldsymbol{\mathcal{N}}}_{mn}\mathbf{w} + \mathbf{c}^{\mathrm{T}}\hat{\boldsymbol{\mathcal{N}}}_{mn}\mathbf{w} + \mathbf{\Phi}^{\mathrm{T}}\boldsymbol{\mathcal{N}}_{mn}\mathbf{w} = \mathbf{P}^{w} \end{cases} \tag{15}$$

The first three equations express the compatibility of membrane strains, while the fourth one is the dynamic equilibrium along the out-of-plane direction. The differential problem of Eq. (15) holds for the case of in-plane movable and immovable edges. When free in-plane edges are considered, the problem reduces to the third and fourth equations, while the amplitudes c_k, d_j are identically zero.

3 Solution procedures

The nonlinear dynamic behavior of VS composite plates can be assessed in terms of frequency–amplitude or time response by solving Eq. (15). In this section, four techniques, each characterized by with different approximations, are proposed, i.e. the method of averaging, a perturbation procedure, an iterative method and a direct time integration approach. The reason for developing various solution strategies is justified by the practical need to have an analysis framework through which the designer can compare different methods and make a choice on the most appropriate one for the specific application. Purpose of this work is providing a systematic comparison of these solution procedures in terms of accuracy, complexity and computation cost, in order to determine in which application field they are more suitable for. To this aim, different problems concerning free and forced nonlinear vibrations of VS plate are illustrated in the successive sections.

3.1 Method of averaging

The first approach deals with the method of averaging. Before introducing the method, the governing equations are re-organized in a more suitable way. Specifically, a static condensation is operated after recalling that the in-plane inertia is neglected. It follows that the stress function amplitudes, i.e. $\mathbf{d}$, $\mathbf{c}$, $\mathbf{\Phi}$, can be expressed as a function of the unknowns $\mathbf{w}$ by formal substitution of the first three of Eq. (15) into the fourth one. One single differential equation, expressing the dynamic equilibrium in the out-of-plane direction, is then obtained as:

$$\mathbf{M}^{ww}\ddot{\mathbf{w}} + \mathbf{K}^{ww}_{\mathrm{L}}\mathbf{w} + \mathbf{K}^{ww}_{\mathrm{NL}_3}\mathbf{w} = \mathbf{P}^{w} \tag{16}$$

where the matrix $\mathbf{K}_{\mathrm{L}}$ denotes the linear stiffness matrix, while $\mathbf{K}_{\mathrm{NL}_3}$ is the stiffness matrix whose nonlinearities are due to the cubic terms in $\mathbf{w}$.

A further reduction of order can be operated by expressing Eq. (16) in terms of modal coordinates. This operation is of particular interest when the low-frequency response is of concern and few modes need to be included in the expansion. By defining the transformation between the Ritz amplitudes and the first r modal coordinates as $\mathbf{w} = \mathbf{V}^{\mathrm{r}}\mathbf{q}$, Eq. (16) transforms into:

$$\ddot{q}_i + c_i\dot{q}_i + k_i q_i + \sum_{j=1}^{r}\sum_{k=1}^{r}\sum_{s=1}^{r} b_{ijks} q_j q_k q_s = p_i \quad \text{for} \quad i = 1, 2, ...r \tag{17}$$

where q_i are the generalized modal coordinates; the coefficients k_i, b_{ijks} and p_i are the projection of $\mathbf{K}_{\mathrm{L}}^{ww}$, $\mathbf{K}_{\mathrm{NL}_3}^{ww}$ and $\mathbf{P}^{w}$ onto the modal basis $\mathbf{V}^{r}$. Note, viscous damping has been introduced in Eq. (17) in the form of modal damping, i.e. $c_i = 2\xi_i\omega_i$, where ξ_i is the damping ratio here assumed equal for each mode r.

Starting from Eq. (17), the method of averaging allows to handle the time dependency through the application of an averaging scheme. This operation permits a simplification of the set of Eq. (17) which can then be solved with reduced effort. The method of averaging is developed by considering a two-mode approximation of the solution. Extensions to larger modal basis can be operated with the same framework, while the single-mode approach can be retrieved as a special case.

Recalling Eq. (17), and taking $r = 2$, one obtains:

$$\begin{cases} \ddot{q}_1 + c_1\dot{q}_1 + \omega_1^2 q_1 + \beta_{1111} q_1^3 + \beta_{1112} q_1^2 q_2 + \beta_{1122} q_1 q_2^2 + \beta_{1222} q_2^3 = p_1 \cos(\omega t) \\ \ddot{q}_2 + c_2\dot{q}_2 + \omega_2^2 q_2 + \beta_{2111} q_1^3 + \beta_{2112} q_1^2 q_2 + \beta_{2122} q_1 q_2^2 + \beta_{2222} q_2^3 = p_2 \cos(\omega t) \end{cases} \tag{18}$$

where $\beta_{1111} = b_{1111}$, $\beta_{1222} = b_{1222}$, $\beta_{2111} = b_{2111}$, $\beta_{2222} = b_{2222}$ and:

$$\begin{aligned} \beta_{1112} &= b_{1112} + b_{1121} + b_{1211} \quad \beta_{1122} = b_{1122} + b_{1221} + b_{1212} \\ \beta_{2112} &= b_{2112} + b_{2121} + b_{2211} \quad \beta_{2122} = b_{2122} + b_{2221} + b_{2212} \end{aligned} \tag{19}$$

The averaged dynamics of the system is derived starting from an assumed solution in form:

$$\begin{cases} q_1(t) = A_1(t)\cos(\chi_1(t)) \\ q_2(t) = A_2(t)\cos(\chi_2(t)) \end{cases} \tag{20}$$

where $\chi_1 = \omega t + \psi_1$ and $\chi_2 = \omega t + \psi_2$. The method relies upon the assumption that the amplitudes and phases are slowly varying function of time, i.e:

$$\begin{cases} \dot{q}_1(t) = -A_1(t)\omega\sin(\chi_1(t)) \\ \dot{q}_2(t) = -A_2(t)\omega\sin(\chi_2(t)) \end{cases} \tag{21}$$

The approximation above can be understood by observing that the linear counterpart of Eq. (18), i.e. the equation obtained by dropping the nonlinear terms, admits solution in the form of Eq. (20), with A_i and ψ_i

independent on time. The underlying idea of the method of averaging is that nonlinear terms will lead the solution to slightly deviate from the linear one, thus resembling Eq. (20), but with amplitudes and phases which are slowly varying functions of time.

Following the procedure described in Ref. [19, 44], it is possible to substitute Eqs. (20) and (21) into Eq. (18), leading to four differential equations involving the unknowns A_i and ψ_i. Successive integration over one period of the motion leads to the averaged equations:

$$
\begin{aligned}
\dot{\overline{\psi}}_1 &= \frac{1}{2\overline{A}_1\omega}[-\overline{A}_1\omega^2 + \overline{A}_1\omega_1^2 + \frac{3}{4}\overline{A}_1^3\beta_{1111} + \frac{3}{4}\overline{A}_1^2\overline{A}_2\beta_{1112}\cos(\overline{\Delta}) + \frac{3}{4}\overline{A}_1\overline{A}_2^2\beta_{1122}\cos^2(\overline{\Delta}) + \\
&+ \frac{3}{4}\overline{A}_2^3\beta_{1222}\cos^3(\overline{\Delta}) + \frac{1}{4}\overline{A}_1\overline{A}_2^2\beta_{1122}\sin^2(\overline{\Delta}) + \frac{3}{4}\overline{A}_2^3\beta_{1222}\cos(\overline{\Delta})\sin^2(\overline{\Delta}) - p_1\cos(\overline{\psi}_1)] \\
\dot{\overline{A}}_1 &= \frac{1}{2\omega}[-\overline{A}_1 c_1\omega - \frac{1}{4}\overline{A}_1^2\overline{A}_2\beta_{1112}\sin(\overline{\Delta}) - \frac{1}{4}\overline{A}_1\overline{A}_2^2\beta_{1122}\sin(2\overline{\Delta}) - \frac{3}{4}A_2^3\beta_{1222}\cos^2(\overline{\Delta})\sin(\overline{\Delta}) + \\
&- \frac{3}{4}A_2^3\beta_{1222}\sin^3(\overline{\Delta}) - p_1\sin(\overline{\psi}_1)] \\
\dot{\overline{\psi}}_2 &= \frac{1}{2\overline{A}_2\omega}[-\overline{A}_2\omega^2 + \overline{A}_2\omega_2^2 + \frac{3}{4}\overline{A}_1^3\beta_{2111}\cos^3(\overline{\Delta}) + \frac{3}{4}\overline{A}_1^3\beta_{2111}\cos(\overline{\Delta})\sin^2(\overline{\Delta}) + \frac{3}{4}\overline{A}_1^2\overline{A}_2\beta_{2112}\cos^2(\overline{\Delta}) + \\
&+ \frac{1}{4}\overline{A}_1^2\overline{A}_2\beta_{2112}\sin^2(\overline{\Delta}) + \frac{3}{4}\overline{A}_1\overline{A}_2^2\beta_{2122}\cos(\overline{\Delta}) + \frac{3}{4}\overline{A}_2^3\beta_{2222} - p_2\cos(\overline{\psi}_2)] \\
\dot{\overline{A}}_2 &= \frac{1}{2\omega}[-\overline{A}_2 c_2\omega + \frac{3}{4}\overline{A}_1^3\beta_{2111}\cos^2(\overline{\Delta})\sin(\overline{\Delta}) + \frac{3}{4}\overline{A}_1^3\beta_{2111}\sin^3(\overline{\Delta}) + \frac{1}{4}\overline{A}_1^2\overline{A}_2\beta_{2112}\sin(2\overline{\Delta}) + \\
&+ \frac{1}{4}\overline{A}_1\overline{A}_2^2\beta_{2122}\sin(\overline{\Delta}) - p_2\sin(\overline{\psi}_2)]
\end{aligned}
\tag{22}
$$

where $\Delta = \psi_1 - \psi_2$ is the offset between the two generalized coordinates, q_1 and q_2, and the overline denotes the average value taken over one period. Note, the integrals leading to Eq. (22) are obtained by introducing the approximation below:

$$
\int_0^{2\pi} \dot{A}_i \, \mathrm{d}\chi_i \approx \dot{\overline{A}}_i 2\pi, \qquad \int_0^{2\pi} \dot{\psi}_i \, \mathrm{d}\chi_i \approx \dot{\overline{\psi}}_i 2\pi \tag{23}
$$

which is motivated by the assumption introduced by Eq. (21): amplitudes and phases are slowly varying functions of time, thus their integral over one period can be approximated with the average value.

The method of averaging allows the steady-state response to be evaluated by setting $\dot{\overline{A}}_i$ and $\dot{\overline{\psi}}_i$ equal to zero [19, 44]. In this case, a set of algebraic equations is obtained, whose solution is obtained via Newton-Raphson iterations.

The free vibration problem can be recovered form Eq. (22) by setting to zero the damping and the forcing contributions, i.e. c_i and p_i.

3.2 Perturbation procedure

The second strategy is a perturbation procedure, which is analogous to the well known Koiter's initial postbuckling theory [45] and corresponds to a similar procedure for nonlinear vibrations introduced by Rehfield in Ref. [24]. This procedure is of interest due to its effectiveness in deriving simple closed-form

solutions for describing the nonlinear response of the structure.

The method can be developed by referring to the variational principle of Eq. (6) and assuming a perturbation expansion in the form:

$$\begin{aligned} w &= \xi w^{(1)} + \xi^2 w^{(2)} + \dots \\ F &= \xi F^{(1)} + \xi^2 F^{(2)} + \dots \end{aligned} \tag{24}$$

where ξ is a small perturbation parameter; the functions $w^{(i)}$ and $F^{(i)}$ of Eq. (24) are the solutions of the i-th order problems obtained by substitution of Eq. (24) into Eq. (6) and by successive collection of terms pre-multiplied by corresponding powers of ξ.

The perturbation expansion is conducted here up to the second-order terms. Furthermore, a single-mode approximation is operated, meaning that vibration modes are assumed to be well-separated. This is generally the case for the plate structures under investigation. The coexistence of multiple modes at the same frequency falls beyond the capability of the present formulation.

Rather than developing the formulation at variational principle level, it is advantageous to perform the expansion after the Ritz approximation is introduced [12]. In particular, the Ritz amplitudes are expressed as:

$$\begin{aligned} \mathbf{d} &= \xi \mathbf{d}^{(1)} + \xi^2 \mathbf{d}^{(2)} + \dots \\ \mathbf{c} &= \xi \mathbf{c}^{(1)} + \xi^2 \mathbf{c}^{(2)} + \dots \\ \mathbf{\Phi} &= \xi \mathbf{\Phi}^{(1)} + \xi^2 \mathbf{\Phi}^{(2)} + \dots \\ \mathbf{w} &= \xi \mathbf{w}^{(1)} + \xi^2 \mathbf{w}^{(2)} + \dots \end{aligned} \tag{25}$$

The first-order problem is derived by substituting Eq. (25) into Eq. (15) and by collecting the linear terms in ξ, leading to:

$$\begin{cases} \mathbf{S}^{dd}\mathbf{d}^{(1)} + \mathbf{S}^{dc}\mathbf{c}^{(1)} + \mathbf{S}^{d\Phi}\mathbf{\Phi}^{(1)} = \mathbf{0} \\ \mathbf{S}^{cd}\mathbf{d}^{(1)} + \mathbf{S}^{cc}\mathbf{c}^{(1)} + \mathbf{S}^{c\Phi}\mathbf{\Phi}^{(1)} = \mathbf{0} \\ \mathbf{S}^{\Phi d}\mathbf{d}^{(1)} + \mathbf{S}^{\Phi c}\mathbf{c}^{(1)} + \mathbf{S}^{\Phi\Phi}\mathbf{\Phi}^{(1)} = \mathbf{0} \\ \mathbf{M}^{ww}\ddot{\mathbf{w}}^{(1)} + \mathbf{K}^{ww}\mathbf{w}^{(1)} = \mathbf{0} \end{cases} \tag{26}$$

The first three equations are identically satisfied by taking $\mathbf{c}^{(1)} = \mathbf{d}^{(1)} = \mathbf{\Phi}^{(1)} = \mathbf{0}$, while the solution of the fourth equation is sought in the form of $\mathbf{w}^{(1)} = \hat{\mathbf{w}}^{(1)} \cos(\omega t)$. The first-order problem is therefore reduced to:

$$\left(-\omega^2 \mathbf{M}^{ww} + \mathbf{K}^{ww}\right) \hat{\mathbf{w}}^{(1)} = \mathbf{0} \tag{27}$$

which is an eigenvalue problem in a standard form. The eigenvector $\hat{\mathbf{w}}^{(1)}$ is conveniently normalized with respect to the thickness h, so that the perturbation parameter ξ can be understood as the nondimensional

amplitude $w_{\max}/h$.

The second-order problem is derived by collecting the quadratic terms in ξ and reads:

$$\begin{cases} \mathbf{S}^{dd}\mathbf{d}^{(2)} + \mathbf{S}^{dc}\mathbf{c}^{(2)} + \mathbf{S}^{d\Phi}\mathbf{\Phi}^{(2)} = -\dfrac{1}{2}{\mathbf{w}^{(1)}}^{\mathrm{T}}\tilde{\boldsymbol{\mathcal{N}}}_j\mathbf{w}^{(1)} \\ \mathbf{S}^{cd}\mathbf{d}^{(2)} + \mathbf{S}^{cc}\mathbf{c}^{(2)} + \mathbf{S}^{c\Phi}\mathbf{\Phi}^{(2)} = -\dfrac{1}{2}{\mathbf{w}^{(1)}}^{\mathrm{T}}\hat{\boldsymbol{\mathcal{N}}}_k\mathbf{w}^{(1)} \\ \mathbf{S}^{\Phi d}\mathbf{d}^{(2)} + \mathbf{S}^{\Phi c}\mathbf{c}^{(2)} + \mathbf{S}^{\Phi\Phi}\mathbf{\Phi}^{(2)} = -\dfrac{1}{2}{\mathbf{w}^{(1)}}^{\mathrm{T}}\boldsymbol{\mathcal{N}}_{pq}\mathbf{w}^{(1)} \\ \mathbf{M}^{ww}\ddot{\mathbf{w}}^{(2)} + \mathbf{K}^{ww}\mathbf{w}^{(2)} = -\left({\mathbf{d}^{(1)}}^{\mathrm{T}}\tilde{\boldsymbol{\mathcal{N}}}_{mn} + {\mathbf{c}^{(1)}}^{\mathrm{T}}\hat{\boldsymbol{\mathcal{N}}}_{mn} + {\mathbf{\Phi}^{(1)}}^{\mathrm{T}}\boldsymbol{\mathcal{N}}_{mn}\right)\mathbf{w}^{(1)} \end{cases} \tag{28}$$

The right-hand side of the first three of Eq. (28) shows that the Airy stress function coefficients can be expressed as $\{\mathbf{d}^{(2)}, \mathbf{c}^{(2)}, \mathbf{\Phi}^{(2)}\} = \{\hat{\mathbf{d}}^{(2)}, \hat{\mathbf{c}}^{(2)}, \hat{\mathbf{\Phi}}^{(2)}\}\cos^2(\omega t)$. Based on this observation, along with substitution of the first-order field into Eq. (28), one obtains:

$$\begin{cases} \mathbf{S}^{dd}\hat{\mathbf{d}}^{(2)} + \mathbf{S}^{dc}\hat{\mathbf{c}}^{(2)} + \mathbf{S}^{d\Phi}\hat{\mathbf{\Phi}}^{(2)} = -\dfrac{1}{2}{\hat{\mathbf{w}}^{(1)}}^{\mathrm{T}}\tilde{\boldsymbol{\mathcal{N}}}_j\hat{\mathbf{w}}^{(1)} \\ \mathbf{S}^{cd}\hat{\mathbf{d}}^{(2)} + \mathbf{S}^{cc}\hat{\mathbf{c}}^{(2)} + \mathbf{S}^{c\Phi}\hat{\mathbf{\Phi}}^{(2)} = -\dfrac{1}{2}{\hat{\mathbf{w}}^{(1)}}^{\mathrm{T}}\boldsymbol{\mathcal{N}}_k\hat{\mathbf{w}}^{(1)} \\ \mathbf{S}^{\Phi d}\hat{\mathbf{d}}^{(2)} + \mathbf{S}^{\Phi c}\hat{\mathbf{c}}^{(2)} + \mathbf{S}^{\Phi\Phi}\hat{\mathbf{\Phi}}^{(2)} = -\dfrac{1}{2}{\hat{\mathbf{w}}^{(1)}}^{\mathrm{T}}\boldsymbol{\mathcal{N}}_{pq}\hat{\mathbf{w}}^{(1)} \\ \mathbf{M}^{ww}\ddot{\hat{\mathbf{w}}}^{(2)} + \mathbf{K}^{ww}\hat{\mathbf{w}}^{(2)} = \mathbf{0} \end{cases} \tag{29}$$

which is a linear system in the unknowns $\hat{\mathbf{d}}^{(2)}$, $\hat{\mathbf{c}}^{(2)}$ and $\hat{\mathbf{\Phi}}^{(2)}$ (from the last of Eq. (29), it is straightforward to conclude that $\hat{\mathbf{w}}^{(2)} = \mathbf{0}$). Note, the nonlinear terms $\boldsymbol{\mathcal{N}}$ are on the right-hand side of the expressions and are multiplied by the Ritz amplitudes $\hat{\mathbf{w}}^{(1)}$, available from the solution of the first-order field.

As outlined in the procedure above, the perturbation approach transforms a complex nonlinear problem into a sequence of two linear problems to be solved, namely Eqs. (27) and (29), whose solution is computed with small effort, thus allowing for a fast assessment of the nonlinear dynamic response of the plate.

Once the solutions of the first and second-order fields are available, one can derive the asymptotic relation between the vibration frequency ω and the perturbation parameter ξ in a very compact form [24][46]:

$$\xi\left(1 - \frac{\omega^2}{\omega_{\mathrm{L}}^2}\right) + A_{\mathrm{d}}\xi^2 + B_{\mathrm{d}}\xi^3 + ... = p\phi_0 \tag{30}$$

where ω_{L} is the linear natural frequency, and the non-dimensional coefficients A_{d} and B_{d} are the dynamic "a-factor" and dynamic "b-factor", respectively, whose expressions read:

$$\begin{aligned} A_{\mathrm{d}} &= \frac{1}{\omega_{\mathrm{L}}^2\Delta_{\mathrm{d}}}\int_0^{2\pi}\frac{3}{2}\mathbf{F}^{(1)}\cdot(\mathbf{w}^{(1)}, \mathbf{w}^{(1)})\,\mathrm{d}\tau \\ B_{\mathrm{d}} &= \frac{1}{\omega_{\mathrm{L}}^2\Delta_{\mathrm{d}}}\int_0^{2\pi}\left[2\mathbf{F}^{(1)}\cdot(\mathbf{w}^{(1)}, \mathbf{w}^{(2)}) + \mathbf{F}^{(2)}\cdot(\mathbf{w}^{(1)}, \mathbf{w}^{(1)})\right]\,\mathrm{d}\tau \end{aligned} \tag{31}$$

and where use is made of the short notation due to Hutchinson and Frauenthal [47]:

$$\mathbf{A}\cdot(\mathbf{B}, \mathbf{C}) = \int_{\mathrm{S}}\left(A_{,yy}B_{,x}C_{,x} + A_{,xx}B_{,y}C_{,y} - A_{,xy}B_{,x}C_{,y} - A_{xy}B_{,y}C_{,x}\right)\,\mathrm{dS} \tag{32}$$

The term p of Eq. (30) defines the load amplitude, whilst ϕ_0 is dependent on the shape of the external pressure load and is expressed as:

$$\phi_0 = \frac{1}{\omega_{\mathrm{L}}^2 \Delta_{\mathrm{d}}} \int_0^{2\pi} \overline{\mathbf{q}} \cdot \mathbf{w}^{(1)} \, \mathrm{d}\tau \tag{33}$$

with the nondimensional time variable defined as $\tau = \omega t$, while the constant Δ_{d} is:

$$\Delta_{\mathrm{d}} = \int_0^{2\pi} \dot{\mathbf{w}}^{(1)^{\mathrm{T}}} \mathbf{D} \dot{\mathbf{w}}^{(1)} \, \mathrm{d}\tau \tag{34}$$

where:

$$\mathbf{D} = \frac{abh\rho}{4} \int_{\overline{S}} \overline{X}_m \overline{Y}_n \overline{X}_{\overline{m}} \overline{Y}_{\overline{n}} \, \mathrm{d}\overline{S} \tag{35}$$

and

$$\overline{\mathbf{q}} = \frac{ab}{4} \int_{\overline{S}} \overline{X}_m \overline{Y}_n \, \mathrm{d}\overline{S} \tag{36}$$

The asymptotic relation for the case of free vibration can be readily obtained by dropping the external force contribution in Eq. (30) and leading to:

$$\frac{\omega_{\mathrm{NL}}^2}{\omega_{\mathrm{L}}^2} = 1 + A_{\mathrm{d}} \xi + B_{\mathrm{d}} \xi^2 + ... \tag{37}$$

where ω_{NL} is the nonlinear natural frequency.

3.3 Iterative procedure

The third strategy relies upon the Harmonic Balance Method [48], which consists in expanding the solution of Eq. (17) via truncated Fourier series as:

$$\mathbf{q}(t) \approx \mathbf{Q}_0 + \sum_{k=1}^{K} \left[\mathbf{Q}_{c-k} \cos(k\omega t) + \mathbf{Q}_{s-k} \sin(k\omega t) \right] \tag{38}$$

where $\mathbf{q}$ is the vector collecting the generalized modal coordinates. Based on a number of preliminary studies, an expansion up to K=5 was found as adequate for most cases of interest. The expression of Eq. (38) can be simplified when free vibrations are of concern. In this case, damping effects are not considered, so sine terms can be removed. Further simplifications can be introduced upon inspection of the type of nonlinearity. For the problems at hand, quadratic nonlinearities are identically zero, while cubic ones are not: it follows that the plate response is expected to be symmetric, and the constant term and even harmonics do not provide, in general, a relevant contribution [20, 31].

Upon substitution of Eq. (38) into Eq. (17) and successive balancing of the harmonics, a system of nonlinear algebraic equations is obtained in the form:

$$\left(-\omega^2 \hat{\mathbf{M}} + \omega \hat{\mathbf{C}} + \hat{\mathbf{K}} + \hat{\mathbf{N}} \right) \hat{\mathbf{x}} = \hat{\mathbf{P}} \tag{39}$$

where ω is the frequency of the forcing term, and the vector of unknown amplitudes reads:

$$\hat{\mathbf{x}} = \left\{ \mathbf{Q}_{c-1},\ \mathbf{Q}_{s-1},\ \mathbf{Q}_{c-3},\ \mathbf{Q}_{s-3},\ \mathbf{Q}_{c-5},\ \mathbf{Q}_{s-5} \right\}^{\mathrm{T}} \tag{40}$$

The expression of the terms $\hat{\mathbf{M}}$, $\hat{\mathbf{C}}$, $\hat{\mathbf{K}}$ and $\hat{\mathbf{P}}$ is not reported here for the sake of conciseness, but is available in the Appendix. The forced response of the plate can be addressed by solution of the nonlinear algebraic equations of Eq. (39); a standard Newton-Raphson procedure can be used for this scope.

The nonlinear (undamped) free vibration problem can be recovered as a special case of Eq. (39), by setting the forcing and the damping terms, i.e. $\hat{\mathbf{P}}$ and $\hat{\mathbf{C}}$, to zero. This operation leads to:

$$\left(-\omega_{\mathrm{NL}}^2 \hat{\hat{\mathbf{M}}} + \hat{\hat{\mathbf{K}}} + \hat{\hat{\mathbf{N}}} \right) \hat{\hat{\mathbf{x}}} = \mathbf{0} \tag{41}$$

where $\hat{\hat{\mathbf{M}}}$, $\hat{\hat{\mathbf{K}}}$, $\hat{\hat{\mathbf{N}}}$ and $\hat{\hat{\mathbf{x}}}$ are derived from Eq. (39) by deleting rows and columns corresponding to sine terms. The problem of Eq. (41) is in the form of a nonlinear eigenvalue problem, where ω_{NL} is the unknown natural frequency to be determined and $\hat{\hat{\mathbf{x}}}$ is the corresponding modal shape.

Two procedures can be considered for solving Eq. (41). The first one consists in taking the vibration amplitude as continuation parameter: after setting its value, an iterative scheme is pursued to obtain the corresponding natural frequency, leading to the approach presented in Ref. [30]. The second approach considers the frequency ω_{NL} as continuation parameter, and the corresponding amplitude is obtained via Newton-Raphson iterations.

The former approach is more suitable for structures whose type of nonlinear response is not known, whether of pure softening, pure hardening or mixed, i.e. hardening-softening or softening-hardening. In these cases, the solution branch can be followed in a more straightforward way using the vibration amplitude as a continuation parameter. At the same time, this approach may suffer from convergence difficulties in the presence of coincident vibration modes or bifurcation points [49]. For the problems investigated here, both strategies can be successfully used as the responses are purely of hardening type.

3.4 Direct time integration

The last strategy is based on directly integrating the set of Eq. (17). The integration is performed numerically using the Newmark-β method consisting in the following step-by-step procedure:

$$(a_1 + a_2 c_i + k_i)\, q_i^{(t+\Delta t)} + b_{ijks} q_j^{(t+\Delta t)} q_k^{(t+\Delta t)} q_s^{(t+\Delta t)} = p_i^{(t)} + (a_1 + a_2 c_i)\, q_i^{(t)} + (a_3 - a_4 c_i)\, \dot{q}_i^{(t)} + (a_5 - a_6 c_i)\, \ddot{q}_i^{(t)} \tag{42}$$

with

$$\begin{aligned} \ddot{q}_i^{(t+\Delta t)} &= a_1 \left(q_i^{(t+\Delta t)} - q_i^{(t)} \right) - a_3 \dot{q}_i^{(t)} - a_5 \ddot{q}_i^{(t)} \\ \dot{q}_i^{(t+\Delta t)} &= a_2 \left(q_i^{(t+\Delta t)} - q_i^{(t)} \right) + a_4 \dot{q}_i^{(t)} + a_6 \ddot{q}_i^{(t)} \end{aligned} \tag{43}$$

and

$$a_1 = \frac{1}{\beta \Delta t^2}, \quad a_2 = \frac{\gamma}{\beta \Delta t}, \quad a_3 = \frac{1}{\beta \Delta t}, \quad a_4 = 1 - \frac{\gamma}{\beta}, \quad a_5 = \frac{1}{2\beta} - 1, \quad a_6 = \Delta t \left(1 - \frac{\gamma}{2\beta}\right) \tag{44}$$

where the time step Δt is chosen equal $T/100$, where T is the period of vibration; the parameters β and γ [50] are taken as 0.25 and 0.5, respectively.

In this work, frequency response (forced response) and backbone (free vibrations) curves are of concern, therefore repeated analyses are needed when referring to a direct integration scheme. In particular, the forced response is assessed by application of a load with frequency ω and integrating Eq. (42) until transient effects are dissipated, and a steady-state solution is found. After recording the maximum deflection $w_{\max}$, the frequency ω is updated (increased or decreased depending on the followed solution branch) and the new steady-state solution calculated. The procedure is repeated until the frequency range of interest is spanned. As it concerns nonlinear free vibrations, backbone curves – reporting the nonlinear natural frequency ω_{NL} versus the amplitude of vibration $w_{\max}$ – are traced with a similar approach, which closely resembles the one often used in experimental procedures [20]. Specifically, the backbone curve is obtained by computing the damped response of the structure for different excitation levels, joinining then the peaks of the corresponding frequency response curves. Note, slight amounts of damping are needed to eliminate transient effects when shifting from one steady-state solution to the other.

4 Results

In this section, the results obtained by application of the four solution methods presented earlier are discussed. A preliminary part is devoted to the comparison against reference results, aiming at verifying the correctness of the formulations and their implementation.

Then, the semi-analytical strategies are exploited to perform parametric studies: the effect of different fiber configurations is assessed along with the potential for improving the nonlinear response of VS plates through elastic tailoring.

In the final part, a comparison is given between the four solution procedures in order to check their field of employ and provide general guidelines in their use for a given application.

The mechanical properties of the materials considered in the next sections are summarized in Table 1.

4.1 Convergence analysis

A preliminary study is conducted to illustrate the convergence of the solution for increasing number of trial functions. For this purpose, a VS composite plate is considered with geometry characterized by $a/b = 1$ and $a/h = 250$. The mechanical properties are those of Material A, and the lamination sequence is $\left[\pm\langle 45|90\rangle\right]_{2s}$. The boundary conditions are CSCS with in-plane immovable edges.

The results of linear free vibration analyses are summarized in Table 2, where the nondimensional parameter $\Omega_{\mathrm{L}} = \omega_{\mathrm{L}} a\sqrt{\rho/E_{22}}$ is reported for an increasing number of functions $M = N$ approximating the plate deflection. Note, for linear vibrations, the out-of-plane behaviour is uncoupled from the in-plane one. Thus, the only unknowns of the problem are the ones associated with the deflected pattern w.

From the results, the fast convergence of the solution can be clearly observed. In this example, frequencies converge from above with monotonic behaviour, although this is not necessarily the case, as surface integrals are carried out numerically. A number of functions equal to $M = N = 6$ suffices for reaching convergence of the first frequency, whereas more terms are generally needed for higher-order modes as spatial halfwave-lengths become smaller and smaller. In any case, a choice of $M = N = 8$ is enough to achieve convergence of the first ten frequencies.

An assessment over the nonlinear frequency parameter $\Omega_{\mathrm{NL}} = \omega_{\mathrm{NL}} a\sqrt{\rho/E_{22}}$ is provided in Table 3. The results are presented by assuming a nondimensional deflection $w_{\max}/h$ equal to 1. The analyses are conducted referring to the perturbation procedure, although the same conclusions reported next hold if the other methods were used. Different runs are repeated by varying separately the number of terms describing the Airy function, $P = Q = S$, and the out-of-plane displacement, $M = N$. It is interesting to observe that the nonlinear frequency increases upon refinement of the approximation for the Airy function. In other words, larger frequencies are obtained due to progressive reduction of the model compliance as the number of functions $P = Q = S$ is increased. With this regard, the force-based description of the in-plane behaviour leads to an opposite convergence trend with respect to what observed for the out-of-plane displacements.

For the example at hand, convergence can be achieved by considering $P = Q = S = 6$, while less functions are needed for $M = N$. This conclusion is not of general validity and is, in general, problem-dependent. In the forthcoming sections, a number of functions $M = N = P = Q = S = 8$ will be retained, unless otherwise specified; this choice proved to be adequate for handling all the test cases discussed.

4.2 Comparison against literature results

The comparison against reference results is presented now to give evidence of the correctness of the proposed formulations. For this scope, two examples are presented for the case of nonlinear free vibrations, while a third one deals with the forced response. For those methods relying upon a modal condensation, see Eq. (17), a number of five modes is taken. This choice is motivated by a number of preliminary convergence analyses, proving this choice to be a good compromise between accuracy and computational efficiency. The only exception regards the method of averaging, which is developed by considering a two-mode solution, as inherent in its derivation outlined in Section 3.1.

Free vibrations

The first example is taken from Ref. [18]. The structure is a thin VS plate with geometry $a/b = 1.5$, $a/h = 480$, mechanical properties as per Material C, and stacking sequence $\left[\langle 135|90\rangle, \langle -90| - 45\rangle, \langle 90|45\rangle, \langle 45|0\rangle\right]_s$. The boundary conditions are those of fully clamped with immovable edges, i.e. CCCC-immovable.

The nonlinear free vibration response is presented in terms of the backbone curve. Specifically, the nondimensional frequency ratio $\Omega_{\mathrm{NL}}/\Omega_{\mathrm{L}}$ – the subscripts L and NL stand for linear and nonlinear, respectively – is plotted against the nondimensional vibration amplitude $w_{\max}/h$. This latter corresponds to the maximum deflection, which is observed at mid-point, i.e. $(\xi, \eta) = (0, 0)$.

Results are generated using the four methods outlined in this paper. The comparison is presented in Figure 2 against numerical simulations conducted with the p-version FEM along with First-Order Shear Deformation Theory (FSDT) [18]. The solution procedure adopted in the referenced work is based on the HBM and an arc-length continuation method. Overall, good agreement is observed between the present and the reference results. A slightly stiffer behaviour – nonlinear frequencies are larger for a given amplitude value – is associated with the results of Ref. [18]. This discrepancy is attributed to the handling of in-plane boundary conditions: the displacement-based formulation of Ref. [18] allows in-plane immovable boundary conditions to be enforced in strong-form; on the contrary, the mixed formulation presented here relies upon a definition of in-plane conditions in an average sense. It follows that the four edges are not exactly fixed in the present models, leading to a milder hardening response. In addition, minor differences can be ascribable to the definition of the fiber orientation. Specifically, the FEM models of Ref. [18] consider the structure as an assembly of finite elements, each characterized by a constant fiber orientation within the element domain. On the contrary, the models developed here account for the fiber curvilinear path through the evaluation of the fiber angles at the integration points.

Another example is presented to verify the correct definition and implementation of different sets of in-plane boundary conditions. With this purpose, a straight fiber composite plate taken from Ref. [51] is considered. The motivation for considering a straight fiber configuration is twofold: firstly, the availability of reference results for VS plates under various boundary conditions is relatively limited; secondly, the capability of the present methods to deal with VS configurations has been already shown in the previous test case, thus the effect of boundary conditions can be assessed irrespective of the distribution of elastic properties.

The configuration under investigation is a cross-ply plate with geometry characterized by the nondimensional ratios $a/b = 1$, $a/h = 100$ and made of Material B. The layup is $\left[0/90/0/90/0\right]$. The flexural boundary conditions are those of simple-support, whilst the in-plane ones include immovable, movable and free edges. The results are summarized in Table 4, where the nonlinear frequency ratios are reported for different values of the maximum nondimensional amplitude $w_{\max}/h$. As one may expect, the effect of constraining the in-plane motion is that of increasing the nonlinear frequency for a given amplitude value. Immovable edges are indeed associated with the largest nondimensional frequencies, while the smallest are achieved for free edges.

This trend is correctly captured here and agrees with the results reported in Ref. [51], which are based on the FEM and FSDT, and are obtained using the HBM and the iterative procedure described in [30]. The percent differences between the present methods and the reference one are very small, reaching a maximum value of 1%.

Forced response

A third example is taken from [52]. A VS plate is considered, whose geometry is defined by $a/b = 1$ and $a/h = 50$. The mechanical properties are those of Material D, and the stacking sequence is $\left[\langle 90|45\rangle, 90\langle 90|45\rangle\right]_s$. The plate is constrained with CCCC-immovable conditions. The analysis deals now with the nonlinear forced response of the plate. A uniform pressure of magnitude $p = 2 \times 10^4 N/m^2$ is considered, while the frequency of excitation is taken in the neighborhood of the fundamental one.

The stable branch of the frequency response plot is presented in Figure 3 by reporting the maximum out-of-plane displacement against the nondimensional frequency of excitation. The comparison regards the four methods developed here and the results provided by Ref. [52], where a model based on the p-version FEM and FSDT is used, whereas the Shooting method applied with HBM is adopted as solution procedure. No damping is considered for all methods, i.e. $\xi_i = 0$, apart from the case of direct integration, requiring a slight amount of damping, $\xi_i = 5 \times 10^{-4}$, to allow transient effects to be dissipated over a sufficient number of periods.

Very close agreement is observed between the semi-analytical methods and the reference results, further demonstrating the correct implementation of the four methods also for forced vibration problems.

Note, the boundary conditions in Ref. [52] are expressed in terms of displacements, and not in average sense, as for the present formulation. For this reason, the discrepancies are smaller in the regions characterized by smaller values of $w_{\max}/h$. Here, the coupling between in-plane and out-of-plane response is smaller and, in turn, even the effect of approximate in-plane boundary conditions is less relevant.

It is interesting to note the different matching between results in the two branches depicted in Figure 3. In the range $\Omega = 0.375 - 0.575$ (upper branch), the displacements are under-predicted with respect to Ref. [52]; the opposite holds true for the lower branch, see range $\Omega = 0.55 - 0.6$. This behaviour is explained by noting two main distinctions between the models and responsible for opposite effects. On one hand, the reference model is inherently more compliant, as it is capable of accounting for shear deformability, while the present ones do not. At the same time, the displacement-based approach of the reference model allows immovable edges conditions to be satisfied exactly, thus providing extra-stiffness with respect to the weak-form description implemented here.

4.3 Parametric studies

In this section, the numerical methods developed herein are exploited to perform parametric studies requiring thousands of repeated nonlinear analyses. This is indeed one of the most interesting features of semi-analytical strategies; this aspect is even more important when VS configurations are of concern and larger design spaces have to be handled. In addition, the availability of efficient methods is particularly useful for gathering insight into the mechanical response of the structure, helping to shed light into the tailoring potential offered by VS configurations.

In the following sections, VS plates are considered with planar dimensions given by $a = b = 300$ mm, thickness $h = 1.2$ mm, and elastic properties as per Material A. The layup is given by the stacking of 8 plies oriented at $\left[\pm\langle T_0|T_1\rangle, 90 \pm \langle T_0|T_1\rangle\right]_s$, thus fulfilling typical requirements of symmetric and balanced laminate.

Linear free vibrations

The first investigation focuses on the linear free vibration response. For this purpose, the contour plots of the frequency parameter Ω_{L} are reported in Figure 4 by varying the fiber angles T_0 and T_1 in the ranges $[0, 90]$ and $[-90, 90]$, respectively. Each single point of the plot corresponds to one eigenvalue analysis. Accordingly, the points lying on the diagonal are representative of a configuration with non-steered fibers. Manufacturing constraints are considered by restricting the analysis to configurations exhibiting a maximum curvature smaller or equal than 3.28 m^{-1} [32]. The assessment is conducted for three different sets of boundary conditions, namely CCCC, CSCS and SSSS, inasmuch the constraints are found to affect both the magnitude and the distribution of the frequency parameters in the design space $T_0 - T_1$.

As seen from Figure 4, the frequencies reach their maximum value for straight-fiber configurations, when the plate is constrained with CSCS and SSSS boundary conditions. In particular, the maximum frequency is achieved for the layups corresponding to $T_0 = T_1 = 0$ and $T_0 = T_1 = 45$, respectively. In these cases, no advantages can be achieved through fiber steering. On the contrary, a fully clamped condition, i.e. CCCC, can benefit from the tailoring of the laminate stiffnesses. Specifically, the maximum value is reached for $T_0 = 72$ and $T_1 = 37$. This conclusion is not of general validity, as different patterns can be obtained if the plate aspect ratio or the stacking sequence are taken into consideration [53].

Nonlinear free vibrations

When assessing the nonlinear response, one quantity of interest is the vibration frequency at a given amplitude. In this regard, one may be interested in its absolute value, Ω_{NL}, or the relative one, $\Omega_{\mathrm{NL}}/\Omega_{\mathrm{L}}$. The former depends on the whole design – bending and membrane stiffnesses – and boundary conditions; the latter highlights the effects of the nonlinear membrane stiffening on the plate response – the bending stiffness

is indeed affecting both the linear and nonlinear behaviour. The two cases are investigated next.

Proceeding as done in the linear case, contour plots are generated for different combinations of the fiber angles T_0 and T_1. A nondimensional vibration amplitude $w_{\max}/h$ equal to 1 is considered. The nonlinear frequency ratio $\Omega_{\mathrm{NL}}/\Omega_{\mathrm{L}}$ is reported in Figure 5, where missing regions are associated with non-manufacturable configurations.

The parametric study is conducted for fully-clamped conditions – shown earlier to allow for potential elastic tailoring –, and different sets of in-plane conditions, i.e. free, movable and immovable edges. The perturbation procedure is used for performing simulations, although the same conclusions could be drawn using the other methods. For the study at hand, the advantages of a computationally efficient method are particularly clear; each single plot requires more than 5,000 nonlinear analyses to be run and the total time required by nonlinear FEM simulations would be of several hours. On the contrary, just few minutes were necessary here for conducting the assessment, the single nonlinear analysis requiring 0.2 seconds, approximately, on a laptop with Intel Core i7 and 32 GB of RAM.

A noticeable difference between the case of free edges, Figure 5(a), and the in-plane constrained ones, i.e. Figures 5(b) and 5(c), can be observed by inspection of Figure 5. As a matter of fact, the presence of in-plane constraints, whether they are movable or immovable, is responsible for an internal membrane force distribution, whose effects on the plate response are similar. The larger values of $\Omega_{\mathrm{NL}}/\Omega_{\mathrm{L}}$ in Figures 5(b) and 5(c) are indeed ascribed to beneficial tensile membrane forces promoting hardening response in the nonlinear field. To further investigate this aspect, the results are reported in Table 5 in terms of maximum absolute and relative nonlinear frequency. The corresponding fiber angles T_0 and T_1 are reported as well. The (absolute) nonlinear frequency depends upon a combined effect of bending and membrane stiffnesses, the former being independent on the in-plane boundary conditions. Therefore, it is not surprising that similar fiber steering is observed in the three cases maximizing Ω_{NL}. At the same time, the immovable condition allows a larger value of frequency to be reached due to the constraint-induced membrane stress distribution.

The situation is different when the relative values $\Omega_{\mathrm{NL}}/\Omega_{\mathrm{L}}$ are of concern, see second column of Table 5. The fiber angles leading to the maximum are now different to each other depending on the in-plane conditions. Indeed, both linear and nonlinear frequencies depend on the bending stiffness, so the ratio $\Omega_{\mathrm{NL}}/\Omega_{\mathrm{L}}$ is a measure of the amount of hardening due to the sole membrane response.

Effect of fiber steering

Further insight into the underlying mechanical behaviour of VS plates is provided by investigation of the effects of fiber steering. Specifically, a parametric study is conducted by investigating the behaviour of a plate with $T_1 = 30$ and T_0 ranging between 10 and 40 with steps of 10 degrees. The boundary conditions are those of fully clamped plate with immovable edges. The backbone curve is reported in Figure 6(a) in terms of nondimensional amplitude versus nondimensional frequency. The curves obtained for the three

configurations do not intersect each other, so the contour patterns in the previous sections are expected not to be altered by different amplitude values.

From Figure 6(a), it can be noted that the structural response is characterized by decreased hardening for increased values of T_0. As mentioned earlier, this effect depends on the internal load paths promoted by different forms of fiber steering. Specifically, the nondimensional membrane resultant $\overline{N}_{xx}$ evaluated at $\xi = 0$ is reported in Figure 6(b), where:

$$\overline{N}_{xx} = N_{xx}/N_{xx,\text{ref}} \tag{45}$$

and $N_{xx,\text{ref}}$ is the maximum membrane force obtained for the straight fiber plate with $T_0 = T_1 = 30$.

The plot of Figure 6(b) illustrates that the configuration with the highest degree of hardening is also the one associated with the most intense tensile force redistribution towards the central portion of the plate. Given the single-halfwave shape of the vibration mode, this region is also the one undergoing the largest deflections. This explains why tensile forces are particularly effective here for increasing the nonlinear frequency. It is then concluded that fiber steering allows hardening effects to be shaped through appropriate tailoring of stiffnesses. It is interesting to note the similarity with respect to buckling problems, where increased bifurcation loads can be achieved through similar force redistribution mechanisms [2, 3].

Effect of boundary conditions

The role of in-plane conditions is investigated referring to a VS plate with layup ($T_0 = 15, T_1 = -10$). The backbone curve is depicted in Figure 7(a) for fully clamped plates subjected to free, movable and immovable conditions. As discussed earlier, the maximum and minimum hardening effects are achieved for immovable and free edges conditions, respectively. The curves of Figure 7(a) allow this conclusion to be generalized to different vibration amplitudes. Even in this case, the mechanical response can be understood by assessment of the internal membrane force distribution. The nondimensional resultant $\overline{N}_{xx}$, defined according to Eq. (45), is plotted in Figure 7(b). The movable and immovable conditions lead to similar distributions, the former characterized by null average value. In both cases, tensile forces are shifted towards the middle region, which is beneficial from an hardening response perspective. Similarly, one can observe that the intensity of the tensile load is the smallest when the edges are free.

The effect of out-of-plane constraints is investigated in Figure 8(a), where the backbone curves are reported for immovable in-plane conditions and different sets of flexural conditions, namely CCCC, CSCS and SSSS. The results demonstrate that stiffer flexural constraints lead to smaller degrees of hardening. At a first glance, this behaviour may seem counter-intuitive, and two aspects should be considered to motivate it. Firstly, for a given vibration amplitude $w_{\max}/h$, the membrane forces are relatively similar in the SSSS and CCCC case, although the latter case is characterized by a much larger storage of bending energy; thus, the relative effect of membrane forces is smaller. Secondly, the deflected pattern for clamped case is characterized

by a shorter halfwave-length. The deflected portion is thus narrower under CCCC conditions with respect to the SSSS case, so the effectiveness of membrane tensile forces to stiffen the structure is reduced to a smaller region of the structure.

4.4 Comparison between methods

The four methods developed in this paper are now compared to furnish understanding into their relative advantages and disadvantages. For this scope, VS plates are considered with two different layups, $\left[\pm\langle 15|-10\rangle, 90 \pm \langle 15|-10\rangle\right]_s$ and $\left[\pm\langle 60|40\rangle, 90 \pm \langle 60|40\rangle\right]_s$. The two laminates were chosen after a preliminary assessment, aiming at highlighting two different dynamic responses, with or without the contribution of super-harmonics, respectively.

The forced vibration response is addressed by considering a uniform pressure with magnitude $p = 10N/m^2$ and forcing frequency in the neighborhood of the fundamental natural frequency. The boundary conditions adopted for the comparison are those of fully clamped plate with immovable edges. Damping is set to zero apart from the direct integration method, where a small amount of damping ($\xi_i = 5 \times 10^{-4}$) is introduced to dissipate transient effects and address the steady-state solution.

The results obtained for the first layup, $\left[\pm\langle 15|-10\rangle, 90 \pm \langle 15|-10\rangle\right]_s$, are summarized in Figure 9. Specifically, the stable portion of the frequency response curve is reported in Figure 9(a); the steady-state solution in the upper branch is presented in Figures 9(b) to 9(d) in terms of time response, phase diagram and Fourier spectrum, by considering a forcing frequency $\Omega/\Omega_{\mathrm{L}} = 1.1$. The close agreement between the predictions available from the four methods is quite clear. Apart from some minor discrepancies, all the curves are nearly identical. By inspection of Figure 9(d), one can note that the response is governed by one single harmonic contribution, which justifies the close matching mentioned earlier.

The same conclusions cannot be extended to those cases where the contribution of super-harmonics is relevant. The following example aims at demonstrating this aspect. Specifically, the second layup, $\left[\pm\langle 60|30\rangle, 90 \pm \langle 60|30\rangle\right]_s$, is now considered, and the results of the analyses are summarized in Figure 10.

Looking at the frequency response plot of Figure 10(a), good agreement between all the results can be noted up to a forcing frequency $\Omega/\Omega_L = 1.04$, approximately. As the frequency of excitation is further increased, a divergence occurs between the iterative and direct integration methods on one hand, and the method of averaging and the perturbation procedure on the other hand. In particular, the two former methods predict a change of slope in the frequency-amplitude plot, which is not captured by the latter two methods. This behaviour is further clarified by the inspection of Figures 10(b) and 10(c), where the time response and the phase diagram are shown for $\Omega/\Omega_L = 1.1$. As seen, the solutions available from the direct integration and the iterative procedure account for the contribution of higher-order harmonics. In contrast to this, the single mode perturbation method and the two-mode version of the method of averaging do not capture this effect due to inherent assumptions introduced in their formulation. Interestingly, when $\Omega/\Omega_L = 1.04$ the

forcing frequency is close to one third of the natural frequency of the fifth mode, i.e. $\Omega \backsimeq \Omega_{L,5}/3$. This excitation determines a super-harmonic resonance where two harmonics, the first and the third, provide a contribution to the dynamic response of the plate. The deviation from a pure harmonic motion, which is due to the presence of the third harmonic, can be clearly seen from Figures 10(b) and 10(c). The Fourier spectrum of Figure 10(d) provides further evidence of this aspect, showing the non-negligible contribution of the higher-order harmonics.

Some general consideration in terms of accuracy and range of applicability can be made from the two examples above.

As observed from the previous examples, the four methods are capable of providing accurate solutions whenever the response is characterized by a simple periodic motion. However, deviations from this state lead to imprecision for the present single mode perturbation method and the two-mode version of the method of averaging. These limitations are not inherent restrictions of these methods, but are a consequence of their formulation. Considering the method of averaging, the problem could be addressed by changing the expression of the assumed solution in Eq. (20) to account for harmonic contributions different from the excitation one. However, such corrections would lead to a more cumbersome analytical results for the averaged equations, Eq. (22). Regarding the perturbation procedure, the effect of higher harmonics could be captured by adopting a higher order perturbation expansion in Eq. (25). This change would result in more dynamic terms in the expansion of the nonlinear frequency Eq. (30), but also in more linear problems to be solved with a consequent increase of the computational time.

Deviations from a pure harmonic motion do not affect the accuracy of the direct time integration and the iterative procedure. Regarding these last two methods, the former does not introduce any restrictions on the frequency content of the motion, as the governing equations are directly integrated in time. The formulation of this solution procedure is very general and can predict accurately any type of response, irrespective of its frequency spectrum. The latter relies upon aprioristic assumptions on the spectral distribution of the motion. This implies that any deviation from the assumed spectral content would lead to errors proportional to the importance of the harmonic contributions neglected. Therefore, the formulation of the iterative procedure is somewhat problem-dependent: the Fourier expansion of the variables has to be chosen on the basis of the problem at hand, which, in turn, leads to different nonlinear algebraic equations to be solved.

In addition to the considerations above, it is important to furnish insights into the computational resources required by the four methods.

The most effective ones are found to be the perturbation procedure and the method of averaging. For the problem at hand, the analysis time on a laptop with Intel i7 and 32 GB RAM is few fraction of seconds, the former method being slightly faster than the latter. The improved time required by the perturbation method is to be searched in the very few operations to be conducted numerically, as most of the governing equations are derived in closed-form through analytical manipulation of the expressions, see Eqs. (30) and

(31). On the contrary, a numerical approach is required in the method of averaging for the solution of the averaged equations of motion.

Regarding the direct time integration and the iterative procedure, the computational times are, in general, one or two orders of magnitude higher than the two solution procedures mentioned earlier. Typical times for a run range from few seconds to few minutes, depending on the number of vibration modes considered. In particular, the computational cost of the iterative procedure depends also on the number of terms retained in the Fourier expansion in Eq. (38), which affects the size of the algebraic problem in Eq. (39). Despite the increased number of unknowns associated with the frequency domain representation of the problem, the nonlinear algebraic problem arising from the iterative procedure can be solved faster than the ordinary differential equations associated with the direct time integration method.

All the considerations above can be extended to nonlinear free vibrations problems. However, two peculiar aspects need to be mentioned for this case. Firstly, much larger time is required by use of the direct integration technique, as repeated analyses are needed to trace the backbone plot, as outlined in 3.4. Secondly, the efficiency of the iterative procedure can, in this case, be improved as the contribution of sine terms is null, see Eq. (41), and the set of equations to be solved is then smaller.

5 Conclusions

The work presented a semi-analytical approach for the nonlinear vibration analysis of variable-stiffness plates. With this purpose, a mixed variational principle was successfully introduced for formulating the problem. One advantage relies in the possibility of formulating the problem with less unknowns with respect to a corresponding displacement-based counterpart. Furthermore, the expression of the functional does not require derivatives of the elastic coefficients to be evaluated, resulting in a much simpler expression with respect to a corresponding strong-form formulation. This principle is then believed to be a useful theoretical tool in the field of variable-stiffness plates nonlinear dynamics. The Ritz method was proposed as the approximation strategy for dealing with the spatial dependence, although other methods could be easily employed. Four procedures were considered for solving the semi-discrete equations in terms of temporal dependence.

The comparison with results from the literature, mainly based on finite element simulations, demonstrated the quality of the semi-analytical predictions that, at the same time, require very small computational effort. To illustrate the potential of the approach, studies were conducted for different curvilinear fiber paths and boundary conditions, where thousands of nonlinear analyses were required. Although conclusions are, in most cases, problem-dependent, the tailoring potential to shape the nonlinear response is clear. As observed, the degree of hardening can be increased (reduced) through adequate design of the internal load paths, with tensile (compressive) forces acting on the mostly deflected regions. In this context, the availability of semi-

analytical methods can support the designer in selecting the fiber paths, as well as investigating the effect of boundary conditions.

Among the four techniques for handling the temporal part, the direct integration technique was found to be the most intensive one from a computational perspective, although it can be useful for generating reference solutions. Therefore, it is not recommended when parametric studies are of concern. Quick studies can be realized by using the perturbation technique, which is the fastest approach among those investigated here and, for this reason, is the recommended one. Its formal elegance as well as the availability of simple closed-form solutions to the problem are an additional advantage. Alternatively, the averaging method is a viable strategy requiring similar computational resources. In the context of the formulations developed here, one restriction of these two formulations relies in their inability to capture the potential contribution due to super-harmonics. In a preliminary assessment, these effects can often be neglected. Whenever this is not the case, and more precise results are needed, the iterative procedure should be employed.

Acknowledgements

The first two authors would like to thank Ministero dell'Istruzione, dell'Università della Ricerca for funding this research under PRIN 2017 program.

6 Data availability

The raw/processed data required to reproduce these findings cannot be shared at this time as the data also forms part of an ongoing study.

References

[1] B.I. Hyman et al. "Exploratory tests on fiber-reinforced plates with circular holes under tension". In: *AIAA Journal* 7.9 (1969), pp. 1820–1821.

[2] R. Olmedo and Z. Gürdal. "Buckling response of laminates with spatially varying fiber orientations". In: 34^{th} *AIAA/ASME/ASCE/AHS/ASC Structures, Structural Dynamics and Material Conference*. La Jolla, CA, Apr. 1993.

[3] Z. Wu et al. "Buckling analysis and optimisation of variable angle tow composite plates". In: *Thin-Walled Structures* 60 (2012), pp. 163–172.

[4] B.H. Coburn, Z. Wu, and P.M. Weaver. "Buckling analysis of stiffened variable angle tow panels". In: *Composite Structures* 111 (2014), pp. 259–270.

[5] A. Alhajahmad, M.M. Abdalla, and Z. Gürdal. "Design tailoring for pressure pillowing using tow-placed steered fibers". In: *Journal of Aircraft* 45.2 (2008), pp. 630–640.

[6] B. Coburn. *Buckling of stiffened variable stiffness panels*. Ph.D. Thesis. University of Bristol, 2015.

[7] A. Pagani and A.R. Sanchez-Majano. "Influence of fiber misalignments on buckling performance of variable stiffness composites using layerwise models and random fields". In: *Mechanics of Advanced Materials and Structures* (2020), pp. 1–16.

[8] A. Pagani and A.R. Sanchez-Majano. "Stochastic stress analysis and failure onset of variable angle tow laminates affected by spatial fibre variations". In: *Composites Part C: Open Access* 4 (2021), pp. 1–12.

[9] B.F. Tatting and Z. Gürdal. "Analysis and design of tow-steered variable stiffness composite laminates". In: *AHS Meeting*. Williamsburg, VA, 30 October–1 November 2001.

[10] Z. Gürdal, B.F. Tatting, and C.K. Wu. "Variable stiffness composite panels: effects of stiffness variation on the in-plane and buckling response". In: *Composites Part A: Applied Science and Manufacturing* 39.5 (2008), pp. 911–922.

[11] G. Raju et al. "Optimal postbuckling design of variable angle tow composite plates". In: *AIAA Journal* 56.5 (2018), pp. 2045–2061.

[12] R. Vescovini et al. "Efficient post-buckling analysis of variable-stiffness plates using a perturbation approach". In: *Thin-Walled Structures* 143 (2019), p. 106211.

[13] H. Akhavan, P. Ribeiro, and M.F.S.F. De Moura. "Large deflection and stresses in variable stiffness composite laminates with curvilinear fibres". In: *International Journal of Mechanical Sciences* 73 (2013), pp. 14–26.

[14] A.V. Duran et al. "Thermal buckling of composite plates with spatial varying fiber orientations". In: *Composite Structures* 124 (2015), pp. 228–235.

[15] R. Vescovini and L. Dozio. "Thermal buckling behaviour of thin and thick variable-stiffness panels". In: *Journal of Composites Science* 2.4 (2018), pp. 1–23.

[16] G. Manickam et al. "Thermal buckling behaviour of variable stiffness laminated composite plates". In: *Materials Today Communications* 16 (2018), pp. 142–151.

[17] C.S. Lopes, Z. Gürdal, and P.P. Camanho. "Variable-stiffness composite panels: Buckling and first-ply failure improvements over straight-fibre laminates". In: *Computers & Structures* 86.9 (2008), pp. 897–907.

[18] P. Ribeiro and H. Akhavan. "Non-linear vibrations of variable stiffness composite laminated plates". In: *Composite Structures* 94.8 (2012), pp. 2424–2432.

[19] D.A. Evensen. *A theoretical and experimental study of the nonlinear flexural vibrations of thin circular rings*. Technical report NTRS-19660003735. NASA, 1965.

[20] M. Amabili. *Nonlinear Vibrations and Stability of Shells and Plates*. Cambridge University Press, 2008.

[21] F. Farbod and M. Amabili. "Non-linear vibrations of shells: A literature review from 2003 to 2013". In: *International Journal of Non-Linear Mechanics* 58 (2014), pp. 233–257.

[22] H.-N. Chu and G. Herrmann. "Influence of large amplitude on free flexural vibrations of rectangular elastic plates". In: *Journal of Applied Mechanics* 23 (1956), pp. 532–540.

[23] D. Hui. "Effects of geometric imperfections on large-amplitude vibrations of rectangular plates with hysteresis damping". In: *Journal of Applied Mechanics* 51 (1984), pp. 216–220.

[24] L.W. Rehfield. "Nonlinear free vibrations of elastic structures". In: *International Journal of Solids and Structures* 9.5 (1973), pp. 581–590.

[25] J. Wedel-Heinen. "Vibration of geometrically imperfect beam and shell structures". In: *International Journal of Solids and Structures* 27.1 (1991), pp. 29–47.

[26] C. Mei. "Finite element displacement method for large amplitude free flexural vibrations of beams and plates". In: *Computers & Structures* 3.1 (1973), pp. 163–174.

[27] Y. Shi, R.Y.Y. Lee, and C. Mei. "Finite element method for nonlinear free vibrations of composite plates". In: *AIAA Journal* 35.1 (1997), pp. 159–166.

[28] L.S. Lau, Y.K. Cheung, and S.Y. Wu. "Nonlinear vibration of thin elastic plates, Part 1: Generalized incremental Hamilton's principle and element formulation". In: *Journal of Applied Mechanics* 51 (1984), pp. 837–844.

[29] C.K. Chiang, C. Mei, and C.E. Gray Jr. "Finite element large-amplitude free and forced vibrations of rectangular thin composite plates". In: *Journal of Vibration and Acoustics* 113 (1991), pp. 309–315.

[30] W. Han and M. Petyt. "Geometrically nonlinear vibration analysis of thin, rectangular plates using the hierarchical finite element method–I: the fundamental mode of isotropic plate". In: *Computers & Structures* 63.2 (1997), pp. 295–308.

[31] P. Ribeiro. "Non-linear free periodic vibrations of variable stiffness composite laminated plates". In: *Nonlinear Dynamics* 70.2 (2012), pp. 1535–1548.

[32] A. Houmat. "Nonlinear free vibration of laminated composite rectangular plates with curvilinear fibers". In: *Composite Structures* 106 (2013), pp. 211–224.

[33] M.K Prabhakara and C.Y. Chia. "Non-linear flexural vibrations of orthotropic rectangular plates". In: *Journal of Sound and Vibration* 52.4 (1977), pp. 511–518.

[34] S.I. Chang, A.K. Bajaj, and C.M. Krousgrill. "Non-linear vibrations and chaos in harmonically excited rectangular plates with one-to-one internal resonance". In: *Nonlinear Dynamics* 4.5 (1993), pp. 433–460.

[35] M. Amabili. "Nonlinear vibrations of rectangular plates with different boundary conditions: theory and experiments". In: *Computers & Structures* 82.31-32 (2004), pp. 2587–2605.

[36] E.L. Jansen. "A comparison of analytical–numerical models for nonlinear vibrations of cylindrical shells". In: *Computers & Structures* 82.31-32 (2004), pp. 2647–2658.

[37] V. Giavotto. "Sulla Meccanica di Pannelli di Strutture Aerospaziali". In: *Memorie dell' Istituto Lombardo - Accademia di Scienze e Lettere* XXV.4 (1966). [Italian].

[38] C. Bisagni and R. Vescovini. "Analytical formulation for local buckling and post-buckling analysis of stiffened laminated panels". In: *Thin-Walled Structures* 47.3 (2009), pp. 318–334.

[39] Z. Wu, G. Raju, and P.M. Weaver. "Postbuckling analysis of variable angle tow composite plates". In: *International Journal of Solids and Structures* 50.10 (2013), pp. 1770–1780.

[40] J.N. Reddy. *Mechanics of Laminated Composite Plates and Shells: Theory and Analysis*. Boca Raton: CRC Press, 2004.

[41] V. Giavotto. "Sulla Meccanica dei Pannelli Anisotropi ed Eterogenei". In: *Memorie dell' Istituto Lombardo - Accademia di Scienze e Lettere* XXV.5 (1969). [Italian].

[42] V. Giavotto. "Variational Theory of Thin Shells and Panels". In: *Meccanica* 1.3-4 (1966), pp. 98–107.

[43] Z. Wu, P.M. Weaver, and G. Raju. "Postbuckling optimisation of variable angle tow composite plates". In: *Composite Structures* 103 (1032013), pp. 34–42.

[44] D.K. Liu. *Non-linear vibrations of imperfect thin-walled cylindrical shells*. Ph.D. Thesis. Tu-Delft, 1988.

[45] W.T. Koiter. *On the Stability of Elastic Equilibrium*. Ph.D. Thesis. [in Dutch]. Tu-Delft, 1945.

[46] E.L. Jansen. "A perturbation method for nonlinear vibrations of imperfect structures: Application to cylindrical shell vibrations". In: *International Journal of Solids and Structures* 45.3-4 (2008), pp. 1124–1145.

[47] J.W. Hutchinson and J.C. Frauenthal. "Elastic postbuckling behavior of stiffened and barreled cylindrical shells". In: *Journal of Applied Mechanics* 36.4 (1969), pp. 784–790.

[48] M.S. Nakhla. "A piecewise harmonic balance technique for determination of periodic response of nonlinear system". In: *IEEE Transactions on Circuits and Systems* 23.2 (1976), pp. 85–91.

[49] P. Ribeiro and M. Petyt. "Non-linear free vibration of isotropic plates with internal resonance". In: *International Journal of Non-linear Mechanics* 35.2 (2000), pp. 263–278.

[50] S.S. Rao. *The Finite Element Method in Engineering*. Burlington, MA, USA: Butterworth-heinemann, 2017.

[51] M.K. Singha. "Nonlinear vibration and dynamic stability analysis of composite plates". In: *Journal of Sound and Vibration* 328.4–5 (2009), pp. 541–554.

[52] H. Akhavan. *Non-linear vibrations of tow placed variable stiffness composite laminates*. Ph.D. Thesis. Universidade do Porto, 2015.

[53] A. Houmat. "Optimal lay-up design of variable stiffness laminated composite plates by a layer-wise optimization technique". In: *Engineering Optimization* 50.2 (2018), pp. 205–217.

[54] C.A. Yan. *Non-linear vibrations of variable stiffness plates using Ritz and perturbation methods*. MSc Thesis. Politecnico di Milano, 2019.

Table 1: Mechanical properties of composite materials.

Material	E_{11} (GPa)	E_{22} (GPa)	G_{12} (GPa)	ν_{12} (-)	ρ (kg/m^3)
A	131.70	9.86	4.21	0.28	1600
B	40.00	1.00	0.50	0.25	1000
C	120.50	9.63	3.58	0.32	1540
D	142.00	10.30	7.20	0.27	1580

Table 2: Convergence study ($M = N$) on the fundamental linear frequency parameter $\Omega_{\mathrm{L}} = \omega_{\mathrm{L}} a\sqrt{\rho/E_{22}}$ of a plate with $a/b = 1$, $a/h = 250$, Material A, layup $\left[\pm\langle 45|90\rangle\right]_{2s}$, and boundary conditions CSCS.

	$\Omega_{\mathrm{L}} \times 10 = \omega_{\mathrm{L}} a\sqrt{\rho/E_{22}} \times 10$			
mode	$M = 4$	$M = 6$	$M = 8$	$M = 10$
1	0.5953	0.5952	0.5952	0.5952
2	1.2090	1.2025	1.2024	1.2024
3	1.5035	1.4985	1.4984	1.4984
4	2.1124	2.0855	2.0821	2.0818
5	2.3233	2.3070	2.3049	2.3047
6	3.0849	3.0366	3.0356	3.0356
7	3.1041	3.0851	3.0724	3.0690
8	3.3695	3.3420	3.3198	3.3149
9	4.1301	4.0410	4.0340	4.0338
10	4.2886	4.2653	4.2322	4.2272

Table 3: Convergence study ($P = Q = S$, $M = N$) for the nonlinear frequency parameter $\Omega_{\mathrm{NL}} = \omega_{\mathrm{NL}} a\sqrt{\rho/E_{22}}$ – VS plate with $a/b = 1$, $a/h = 250$, Material A, layup $\left[\pm\langle 45|90\rangle\right]_{2s}$ and boundary conditions CSCS with immovable edges.

	$\Omega_{\mathrm{NL}} \times 10^2 = \omega_{\mathrm{NL}} a\sqrt{\rho/E_{22}} \times 10^2$			
$w_{\max}/h = 1$	$P = 4$	$P = 6$	$P = 8$	$P = 10$
$M = 4$	7.4129	7.4409	7.4428	7.4432
$M = 5$	7.4137	7.4418	7.4437	7.4440
$M = 6$	7.4134	7.4414	7.4433	7.4436
$M = 7$	7.4134	7.4414	7.4433	7.4436

Table 4: Nonlinear frequency ratio $\Omega_{\mathrm{NL}}/\Omega_{\mathrm{L}}$ for different vibration amplitudes $w_{\max}/h$ and boundary conditions – Composite plate with $a/b = 1$, $a/h = 100$, Material B and layup $\left[0/90/0/90/0\right]$.

$w_{\max}/h$	Method of averaging	Perturbation procedure	Iterative procedure	Direct time integration	Ref. [51]
SSSS-Completely free					
0.2	1.00104	1.00106	1.00104	1.00101	1.00121
0.4	1.00418	1.00424	1.00417	1.00381	1.00482
0.6	1.00937	1.00952	1.00936	1.00850	1.01079
0.8	1.01657	1.01686	1.01865	1.01521	1.01906
1.0	1.02574	1.02622	1.02567	1.02408	1.02952
SSSS-Movable					
0.2	1.01055	1.01069	1.01054	1.01238	1.01057
0.4	1.04157	1.04210	1.04159	1.04232	1.04169
0.6	1.09139	1.09246	1.09147	1.08924	1.09167
0.8	1.15771	1.15929	1.15790	1.15256	1.15823
1.0	1.23805	1.23993	1.23839	1.23168	1.23885
SSSS-Immovable					
0.2	1.03160	1.03199	1.03161	1.02948	1.03147
0.4	1.12141	1.12253	1.12151	1.11865	1.12099
0.6	1.25784	1.25905	1.25828	1.24369	1.25723
0.8	1.42858	1.42841	1.42973	1.41971	1.42805
1.0	1.62373	1.62036	1.62601	1.63309	1.62368

Table 5: Optimal lamination configurations (T_0, T_1) for the nonlinear frequency parameter Ω_{NL} and frequency ratio $\Omega_{\mathrm{NL}}/\Omega_{\mathrm{L}}$ for amplitude of vibration $w_{\max}/h = 1$ considering different boundary conditions.

	Max Ω_{NL}		Max $\Omega_{\mathrm{NL}}/\Omega_{\mathrm{L}}$	
Boundary condition	(T_0, T_1)	Ω_{NL}	(T_0, T_1)	$\Omega_{\mathrm{NL}}/\Omega_{\mathrm{L}}$
CCCC-Completely free	(83,44)	0.1122	(9,37)	1.0601
CCCC-Movable	(86,46)	0.1130	(90,90)	1.0850
CCCC-Immovable	(83,44)	0.1247	(14,-14)	1.1812

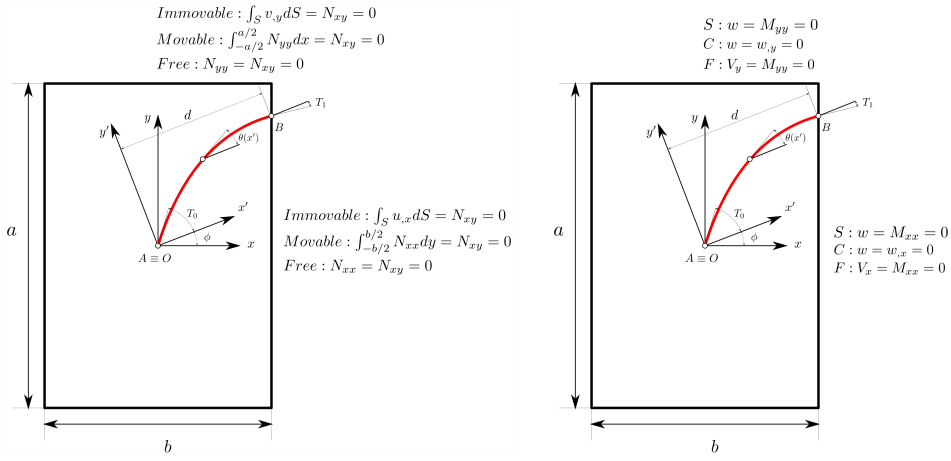

Figure 1: Fiber path, plate geometry and boundary conditions: (a) in-plane, (b) flexural.

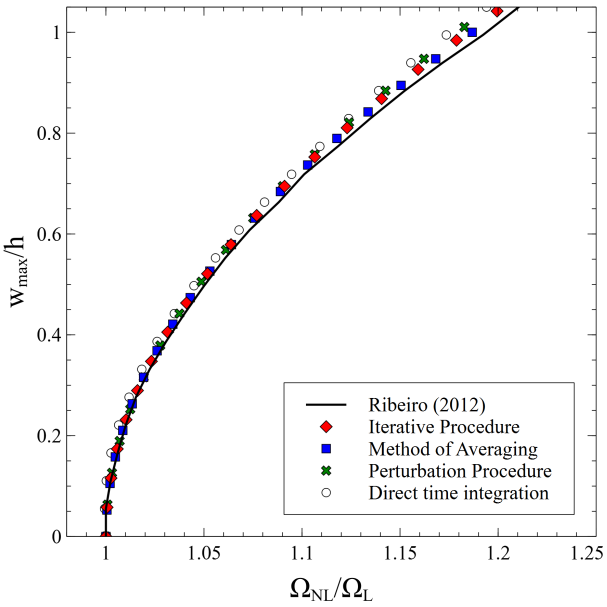

Figure 2: Backbone curves using different methods – $a/b = 1.5$, $a/h = 480$, Material C and layup $\left[\langle 135|90\rangle, \langle -90|-45\rangle, \langle 90|45\rangle, \langle 45|0\rangle\right]_s$.

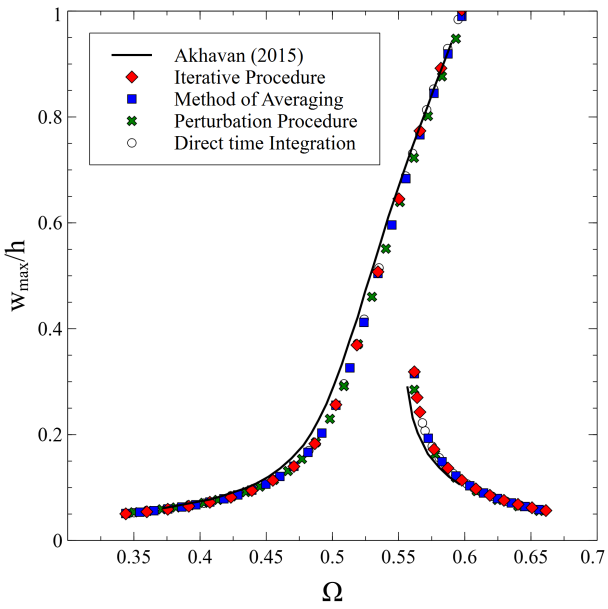

Figure 3: Frequency response plot using different methods – $a/b = 1$, $a/h = 50$, Material D, layup $\left[\langle 90|45\rangle, 90\langle 90|45\rangle\right]_s$, boundary conditions CCCC-immovable, uniform pressure load load ($p = 2 \times 10^4$ Pa).

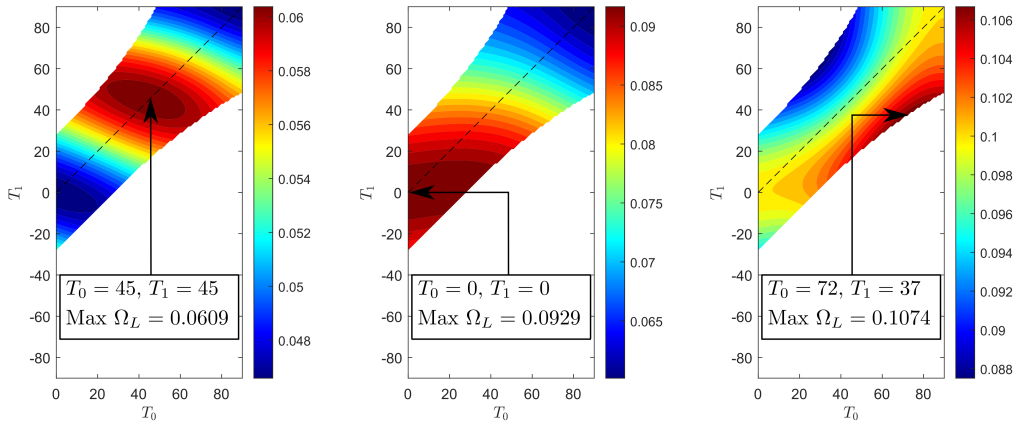

(a) (b) (c)

Figure 4: Contour plots of the linear frequency parameter Ω_{L} – $a = b = 300$ mm, $h = 1.2$ mm, Material A and layup $\left[0 \pm \langle T_0 | T_1 \rangle, 90 \pm \langle T_0 | T_1 \rangle\right]_s$: (a) SSSS, (b) CSCS, (c) CCCC.

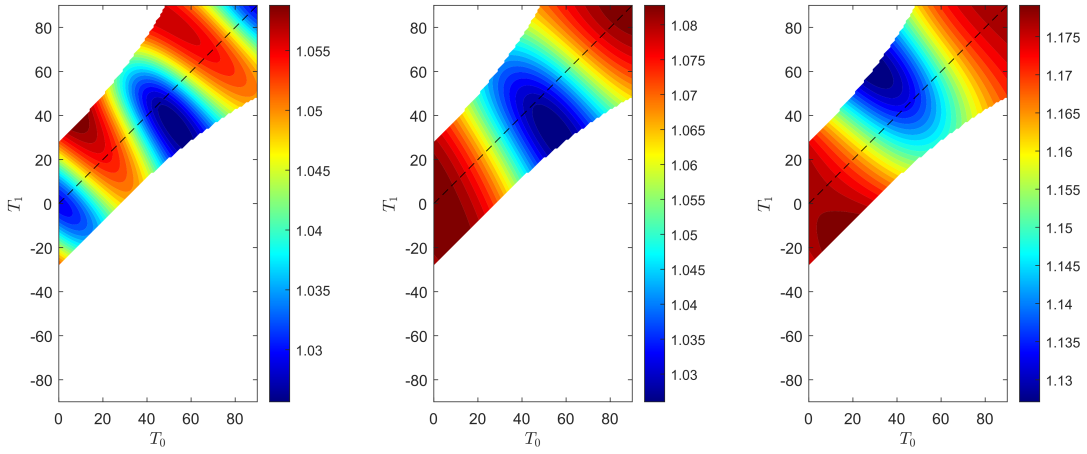

(a) (b) (c)

Figure 5: Contour plots of the frequency ratio $\Omega_{\mathrm{NL}}/\Omega_{\mathrm{L}}$ – $a = b = 300$ mm, $h = 1.2$ mm, Material A and layup $\left[0 \pm \langle T_0|T_1\rangle, 90 \pm \langle T_0|T_1\rangle\right]_s$: (a) CCCC-completely free, (b) CCCC-movable, (c) CCCC-immovable.

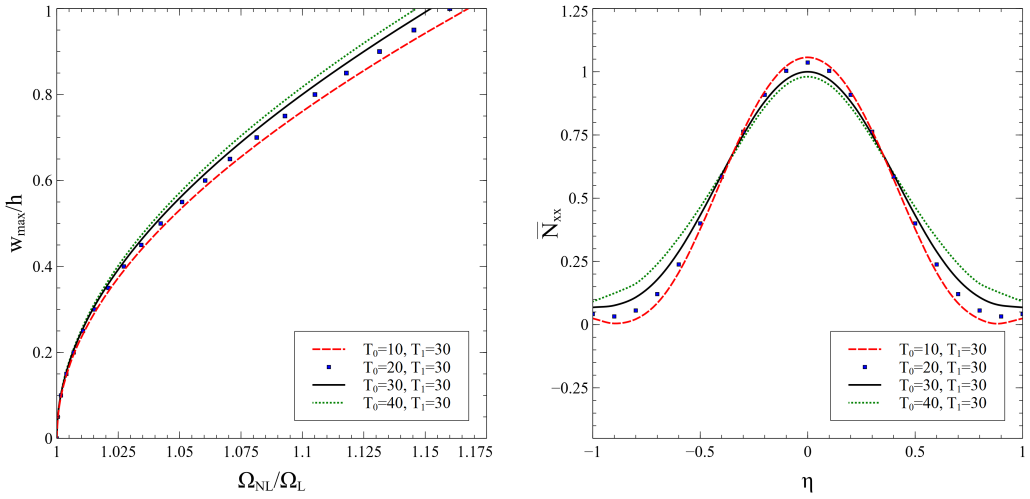

(a) (b)

Figure 6: Effect of the angle T_0 on nonlinear free vibrations – $a = b = 300$ mm, $h = 1.2$ mm, Material A, layup $\left[0 \pm \langle T_0|T_1\rangle, 90 \pm \langle T_0|T_1\rangle\right]_s$ and CCCC-immovable boundary conditions: (a) backbone curve, (b) in-plane resultant $\overline{N}_{xx}$ at $\xi = 0$.

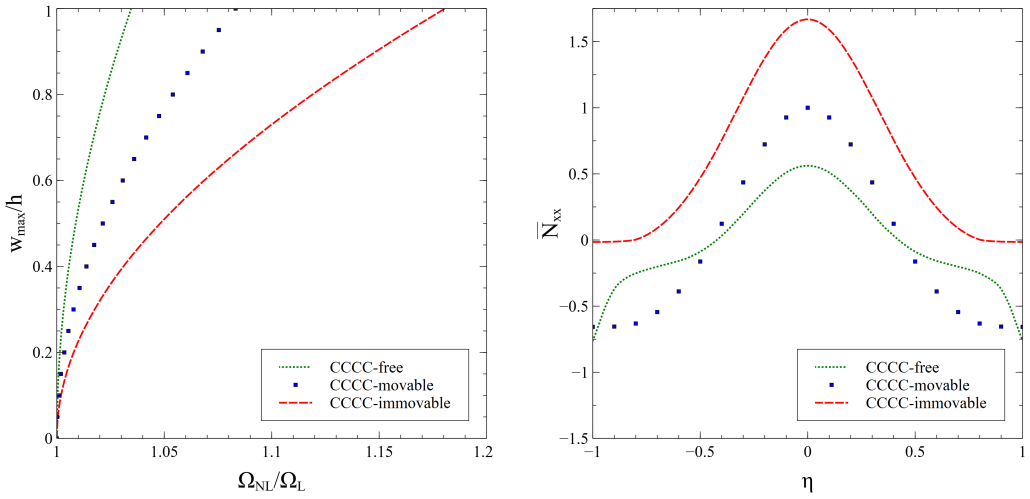

(a) (b)

Figure 7: Effect of in-plane boundary conditions on free vibrations – $a = b = 300$ mm, $h = 1.2$ mm, Material A, layup $\left[0 \pm \langle 15| - 10\rangle, 90 \pm \langle 15| - 10\rangle\right]_s$ and CCCC boundary conditions: (a) backbone curve, (b) in-plane resultant $\overline{N}_{xx}$ at $\xi = 0$.

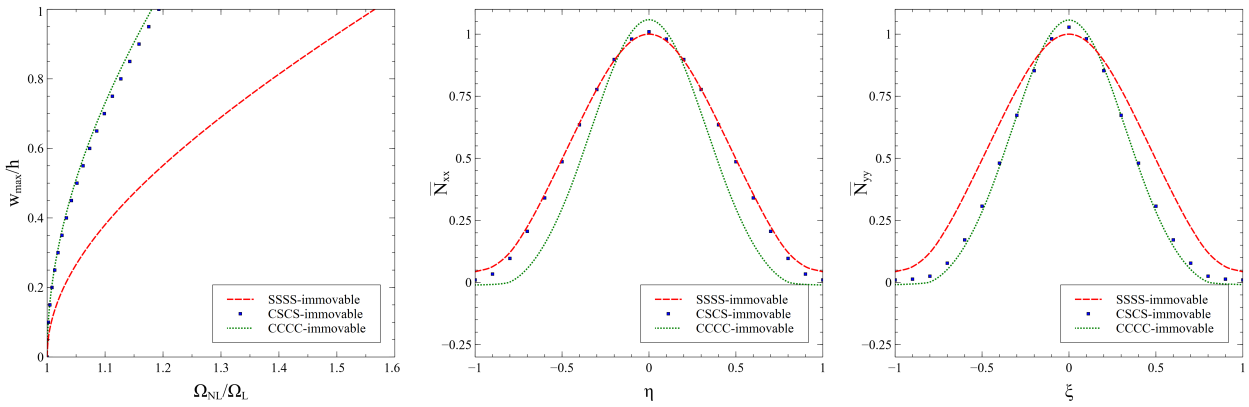

(a) (b) (c)

Figure 8: Effect of out-plane boundary conditions on free vibrations – $a = b = 300$ mm, $h = 1.2$ mm, Material A, layup $\left[0 \pm \langle 15| - 10\rangle, 90 \pm \langle 15| - 10\rangle\right]_s$ and immovable edges: (a) backbone curve, (b) in-plane resultant $\overline{N}_{xx}$ at $\xi = 0$, (c) in-plane resultant $\overline{N}_{yy}$ at $\eta = 0$.

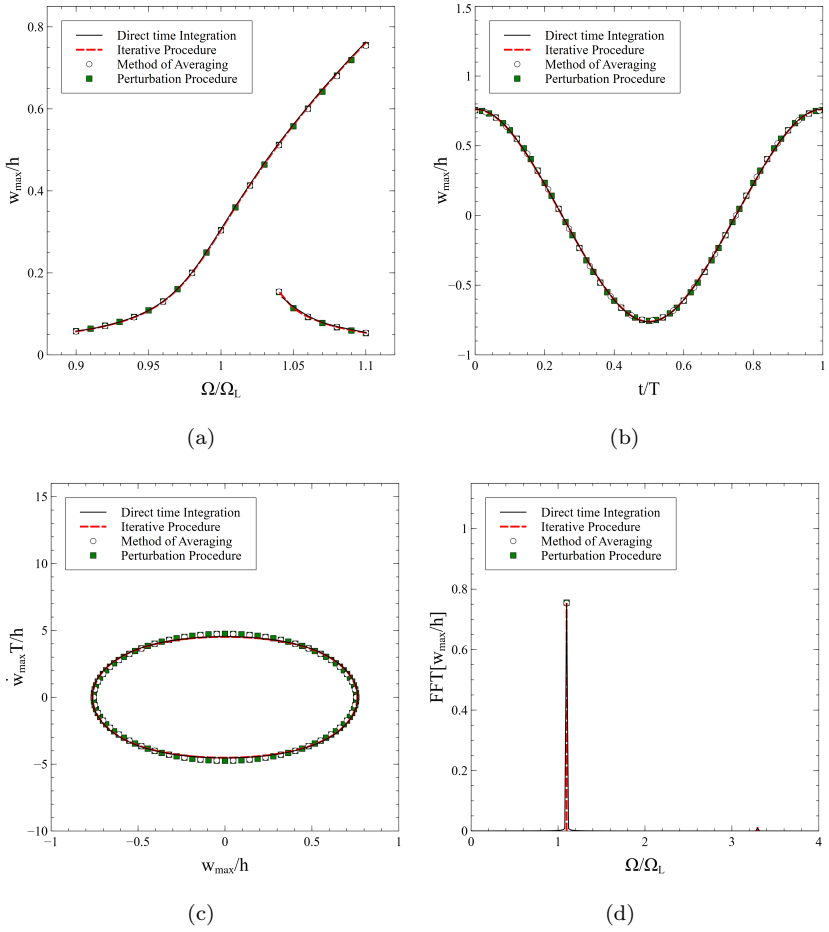

Figure 9: Comparison between methods – $a = b = 300$ mm, $h = 1.2$ mm, Material A, layup $\left[0 \pm \langle 15| - 10\rangle, 90 \pm \langle 15| - 10\rangle\right]_s$, boundary conditions CCCC-immovable, uniform pressure load load (p=10 Pa): (a) frequency response curve, (b) time-domain response, (c) phase plane diagram and (d) Fourier spectrum for forcing frequency Ω=1.1Ω_{L}.

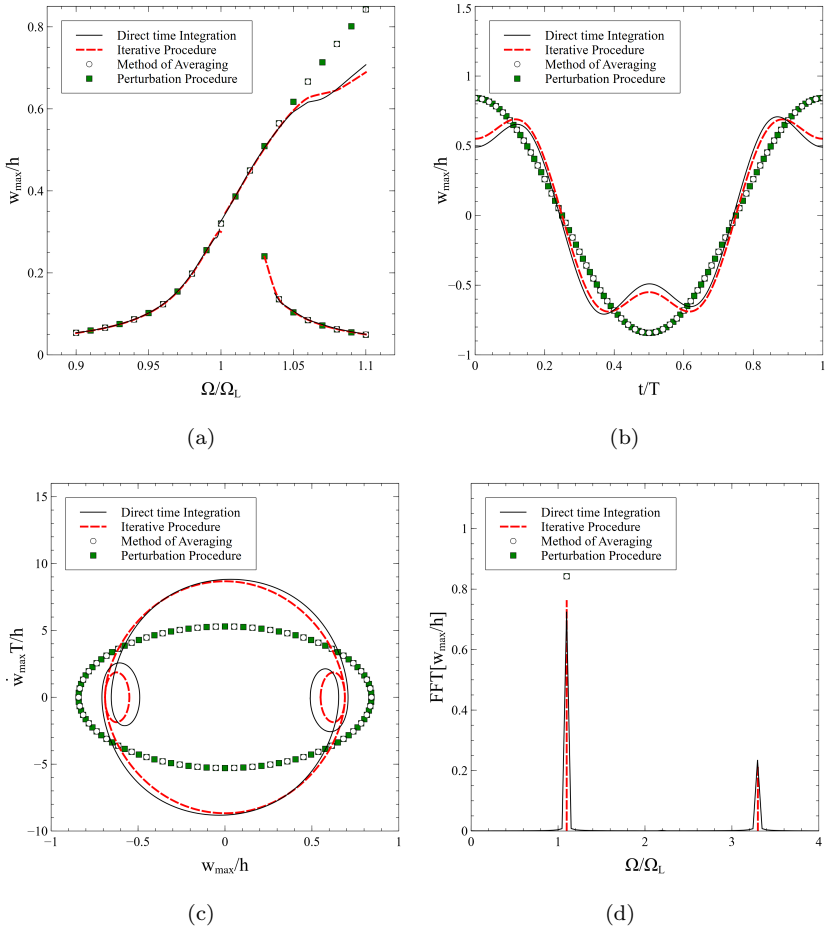

Figure 10: Comparison between methods – $a = b = 300$ mm, $h = 1.2$ mm, Material A, layup $\left[0 \pm \langle 60|40\rangle, 90 \pm \langle 60|40\rangle\right]_s$, boundary conditions CCCC-immovable, uniform pressure load (p=10 Pa): (a) frequency response curve, (b) time domain response, (c) phase plane diagram and (d) Fourier spectrum for forcing frequency Ω=1.1Ω_{L}.

7 Appendix

The full expression of the integrals of Eq. (6) is:

$$S^{dd}_{(j)(\overline{j})} = \mathbf{S}^{dd} = -\int_{\overline{\mathrm{S}}} a_{22} L_j L_{\overline{j}} \mathrm{d}\overline{\mathrm{S}} \tag{46}$$

$$S^{cc}_{(k)(\overline{k})} = \mathbf{S}^{cc} = -\int_{\overline{\mathrm{S}}} r^4 a_{11} L_k L_{\overline{k}} \mathrm{d}\overline{\mathrm{S}} \tag{47}$$

$$\begin{aligned} S^{\phi\phi}_{(pq)(\overline{pq})} = \mathbf{S}^{\phi\phi} = -\int_{\overline{\mathrm{S}}} \Big[& r^4 a_{11} X_p Y_q'' X_{\overline{p}} Y_{\overline{q}}'' + r^2 a_{12} \left(X_p'' Y_q X_{\overline{p}} Y_{\overline{q}}'' + X_p Y_q'' X_{\overline{p}}'' Y_{\overline{q}} \right) + \\ & + a_{22} X_p'' Y_q X_{\overline{p}}'' Y_{\overline{q}} + r^2 a_{66} X_p' Y_q' X_{\overline{p}}' Y_{\overline{q}}' - r^3 a_{16} \left(X_p Y_q'' X_{\overline{p}}' Y_{\overline{q}}' + X_p' Y_q' X_{\overline{p}} Y_{\overline{q}}'' \right) + \\ & - r a_{26} \left(X_p'' Y_q X_{\overline{p}}' Y_{\overline{q}}' + X_p' Y_q' X_{\overline{p}}'' Y_{\overline{q}} \right) \Big] \mathrm{d}\overline{\mathrm{S}} \end{aligned} \tag{48}$$

$$\begin{aligned} K^{ww}_{(mn)(\overline{mn})} = \mathbf{K}^{ww} = -\int_{\overline{\mathrm{S}}} \Big[& D_{11} \overline{X}_m'' \overline{Y}_n \overline{X}_{\overline{m}}'' \overline{Y}_{\overline{n}} + r^2 D_{12} \left(\overline{X}_m'' \overline{Y}_n \overline{X}_{\overline{m}} \overline{Y}_{\overline{n}}'' + \overline{X}_m \overline{Y}_n'' \overline{X}_{\overline{m}}'' \overline{Y}_{\overline{n}} \right) + \\ & + r^4 D_{22} \overline{X}_m \overline{Y}_n'' \overline{X}_{\overline{m}} \overline{Y}_{\overline{n}}'' + 4 r^2 D_{66} \overline{X}_m' \overline{Y}_n' \overline{X}_{\overline{m}}' \overline{Y}_{\overline{n}}' + \\ & + 2 r D_{16} \left(\overline{X}_m'' \overline{Y}_n \overline{X}_{\overline{m}}' \overline{Y}_{\overline{n}}' + \overline{X}_m' \overline{Y}_n' \overline{X}_{\overline{m}}'' \overline{Y}_{\overline{n}} \right) + \\ & + 2 r^3 D_{26} \left(\overline{X}_m \overline{Y}_n'' \overline{X}_{\overline{m}}' \overline{Y}_{\overline{n}}' + \overline{X}_m' \overline{Y}_n' \overline{X}_{\overline{m}} \overline{Y}_{\overline{n}}'' \right) \Big] \mathrm{d}\overline{\mathrm{S}} \end{aligned} \tag{49}$$

$$S^{cd}_{(k)(j)} = \mathbf{S}^{cd} = -\int_{\overline{\mathrm{S}}} r^2 a_{12} L_k L_j \mathrm{d}\overline{\mathrm{S}} \tag{50}$$

$$S^{\Phi d}_{(pq)(j)} = \mathbf{S}^{\Phi d} = -\int_{\overline{\mathrm{S}}} \left(r^2 a_{12} X_p Y_q'' L_j + a_{22} X_p'' Y_q L_j - r a_{26} X_p' Y_q' L_j \right) \mathrm{d}\overline{\mathrm{S}} \tag{51}$$

$$S^{\Phi c}_{(pq)(k)} = \mathbf{S}^{\Phi c} = -\int_{\overline{\mathrm{S}}} \left(r^4 a_{11} X_p Y_q'' L_k + r^2 a_{12} X_p'' Y_q L_k - r^3 a_{16} X_p' Y_q' L_k \right) \mathrm{d}\overline{\mathrm{S}} \tag{52}$$

$$\tilde{\mathcal{N}}_{(j)(mn)(\overline{mn})} = \tilde{\boldsymbol{\mathcal{N}}}_j = r^2 \int_{\overline{\mathrm{S}}} L_j \overline{X}_m \overline{Y}_n' \overline{X}_{\overline{m}} \overline{Y}_{\overline{n}}' \mathrm{d}\overline{\mathrm{S}} \tag{53}$$

$$\hat{\mathcal{N}}_{(k)(mn)(\overline{mn})} = \hat{\boldsymbol{\mathcal{N}}}_k = r^2 \int_{\overline{\mathrm{S}}} L_k \overline{X}_m' \overline{Y}_n \overline{X}_{\overline{m}}' \overline{Y}_{\overline{n}} \mathrm{d}\overline{\mathrm{S}} \tag{54}$$

$$\mathcal{N}_{(pq)(mn)(\overline{mn})} = \boldsymbol{\mathcal{N}}_{pq} = r^2 \int_{\overline{\mathrm{S}}} \Big[X_p Y_q'' \overline{X}'_m \overline{Y}_n \overline{X}'_{\overline{m}} \overline{Y}_{\overline{n}} - \Big(X'_p Y'_q \overline{X}'_m \overline{Y}_n \overline{X}_{\overline{m}} \overline{Y}'_{\overline{n}} + X'_p Y'_q \overline{X}_m \overline{Y}'_n \overline{X}'_{\overline{m}} \overline{Y}_{\overline{n}} \Big) + + X''_p Y_q \overline{X}_m \overline{Y}'_n \overline{X}_{\overline{m}} \overline{Y}'_{\overline{n}} \Big] \mathrm{d}\overline{\mathrm{S}} \tag{55}$$

$$M^{ww}_{(mn)(\overline{mn})} = \mathbf{M}^{ww} = \frac{a^4 \rho h}{16} \int_{\overline{\mathrm{S}}} \overline{X}_m \overline{Y}_n \overline{X}'_{\overline{m}} \overline{Y}'_{\overline{n}} \mathrm{d}\overline{\mathrm{S}} \tag{56}$$

$$P^{w}_{(mn)} = \mathbf{P}^{w} = \frac{a^4 p}{16} \int_{\overline{\mathrm{S}}} \overline{X}_m \overline{Y}_n \mathrm{d}\overline{\mathrm{S}} \tag{57}$$

The matrix expressions implied by Eq. (39) are defined as:

$$\hat{\mathbf{M}} = \mathrm{diag}(\mathbf{I},\ \mathbf{I},\ 9\mathbf{I}, 9\mathbf{I},\ 25\mathbf{I},\ 25\mathbf{I})$$

$$\hat{\mathbf{K}} = \mathrm{diag}(\mathbf{K}_\mathrm{L},\ \mathbf{K}_\mathrm{L},\ \mathbf{K}_\mathrm{L},\ \mathbf{K}_\mathrm{L},\ \mathbf{K}_\mathrm{L},\ \mathbf{K}_\mathrm{L})$$

$$\hat{\mathbf{C}} = \begin{bmatrix} \mathbf{0} & \mathbf{C} & \mathbf{0} & \mathbf{0} & \mathbf{0} & \mathbf{0} \\ -\mathbf{C} & \mathbf{0} & \mathbf{0} & \mathbf{0} & \mathbf{0} & \mathbf{0} \\ \mathbf{0} & \mathbf{0} & \mathbf{0} & 3\mathbf{C} & \mathbf{0} & \mathbf{0} \\ \mathbf{0} & \mathbf{0} & -3\mathbf{C} & \mathbf{0} & \mathbf{0} & \mathbf{0} \\ \mathbf{0} & \mathbf{0} & \mathbf{0} & \mathbf{0} & \mathbf{0} & 5\mathbf{C} \\ \mathbf{0} & \mathbf{0} & \mathbf{0} & \mathbf{0} & -5\mathbf{C} & \mathbf{0} \end{bmatrix}$$

$$\hat{\mathbf{P}} = \Big\{ \mathbf{P},\ \mathbf{0},\ \mathbf{0},\ \mathbf{0},\ \mathbf{0},\ \mathbf{0} \Big\}^{\mathrm{T}}$$

where $\mathbf{I}$ denotes the identity matrix, $\mathbf{K}_\mathrm{L}$ and $\mathbf{C}$ are diagonal matrices collecting the linear stiffness and the damping coefficients, k_i and c_i, respectively; $\mathbf{P}$ is the vector collecting the forcing terms p_i of Eq. (39). The matrix $\hat{\mathbf{N}}$ is obtained after balancing the harmonics due to nonlinear contributions. The full is available is Ref. [54] and is not reported here for the sake of brevity.